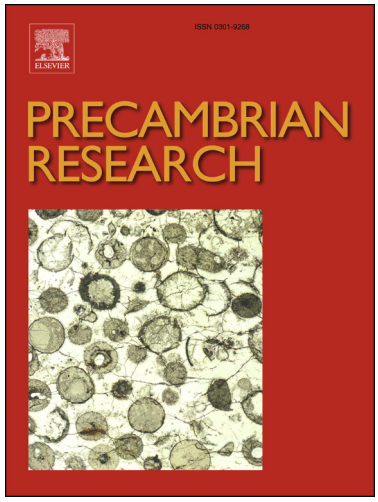

Processes of Crust Formation in the Early Earth Imaged through Hf isotopes from the East Pilbara Terrane

Nicholas J. Gardiner, Arthur H. Hickman, Christopher L. Kirkland, Yongjun Lu, Tim Johnson, Jian-Xin Zhao

PII: S0301-9268(16)30579-4
DOI: http://dx.doi.org/10.1016/j.precamres.2017.05.004
Reference: PRECAM 4764

To appear in: *Precambrian Research*

Received Date: 22 December 2016
Revised Date: 2 May 2017
Accepted Date: 21 May 2017

Please cite this article as: N.J. Gardiner, A.H. Hickman, C.L. Kirkland, Y. Lu, T. Johnson, J-X. Zhao, Processes of Crust Formation in the Early Earth Imaged through Hf isotopes from the East Pilbara Terrane, *Precambrian Research* (2017), doi: http://dx.doi.org/10.1016/j.precamres.2017.05.004

Processes of Crust Formation in the Early Earth Imaged through Hf isotopes from the East Pilbara Terrane

Nicholas J Gardiner[1,2,3], Arthur H Hickman[4], Christopher L Kirkland[1,2,3], Yongjun Lu[4], Tim Johnson[2] and Jian-Xin Zhao[5]

1. Centre for Exploration Targeting – Curtin Node, Department of Applied Geology, Western Australian School of Mines, Curtin University, Perth, WA 6102, Australia.

2. The Institute for Geoscience Research (TIGeR), Department of Applied Geology, Curtin University, GPO Box U1987, Perth WA 6845, Australia.

3. Australian Research Council Centre of Excellence for Core to Crust Fluid Systems, Australia.

4. Geological Survey of Western Australia, 100 Plain Street, East Perth, WA 6004, Australia.

5. Radiogenic Isotope Facility, School of Earth Sciences, The University of Queensland, Brisbane, QLD 4072, Australia

*Correspondence to: nicholas.gardiner@curtin.edu.au

Abstract

The Pilbara Craton, Western Australia, is one of the best preserved Palaeo- to Mesoarchaean terrains on Earth. The East Pilbara Terrane is the archetypical granite-greenstone belt, the dome-like complexes of which were formed through three major magmatic events. These granite domes are comprised of metamorphosed granitic igneous rocks that exhibit a magmatic evolution from early tonalite-trondhjemite-granodiorite (TTG) rocks towards K-rich granites over the period 3.53–2.83 Ga. Accordingly, East Pilbara has been a focus for workers seeking to constrain early Archaean geodynamic processes. One way to inform on this debate is to interrogate successive igneous supersuites using tools sensitive to magmatic source. We present new zircon Hf and whole-rock Nd isotope data from four major supersuites of the Mount Edgar Dome, of the East Pilbara Terrane. Early ca. 3.45 Ga TTGs exhibit isotopic signatures that imply their partial derivation from existing crust, with addition of some juvenile material. Subsequent Palaeoarchaean magmatic events show a secular trend towards more evolved isotopic signatures, interpreted as a dominance of increasing reworking of existing crust, with only minor addition of new juvenile crust. The implication of this is that these later Palaeoarchaean supersuites were largely derived from the melting of older granitic crust, with mass balance modelling suggesting an input of ca. 20% juvenile (depleted mantle) material. The limited addition of juvenile material and increased reworking of existing crust with time, does not support a model of modern-style subduction, but is consistent with vertical tectonic processes in a volcanic plateau-type setting for the East Pilbara Terrane > 3.2 Ga. All Palaeoarchaean Mount Edgar

samples resolve to two-stage Hf model ages of ca. 3.7 Ga and Nd model ages of ca. 3.6 Ga. These Eoarchaean model ages support the existence of a cryptic pre-3.5 Ga protocrust, albeit of unknown extent. Analysis of late Mesoarchaean granites yields highly evolved Hf isotope signatures, consistent with a ca. < 3.2 Ga switch within the Mount Edgar Granitic Complex from dominantly sodic TTG type magmatism towards more K-rich granites as the craton stabilized.

Keywords

Pilbara Craton; Hf Isotopes; Archaean; TTG; Crustal Evolution; Sagduction

1. Introduction

The Pilbara Craton in Western Australia is one of the best preserved Palaeo- to Mesoarchaean terrains on Earth (Barley et al., 1998; Cloud, 1988; Van Kranendonk et al., 2007b). Lying within its northern half, the East Pilbara Terrane (EPT) is its well-preserved Palaeoarchaean section (Fig. 1), for which zircon U-Pb crystallization ages record crustal magmatism spanning 3.53 to 3.22 Ga (Hickman and Van Kranendonk, 2012). Previous workers have interpreted the EPT to have been formed above an extensive substrate as old as 3.70 Ga on the basis of both inherited U-Pb zircon ages, and whole-rock Sm-Nd model ages (Kemp et al., 2015; Van Kranendonk et al., 2007b), with evidence of local older crust of at least ca. 3.80 Ga (Hickman and Van Kranendonk, 2012). Accordingly, the EPT has been a focus for understanding early Earth processes, including Palaeoarchaean crust formation and stabilization, with implications for prevailing geodynamic styles during the early Earth, and the transition to “modern-style” plate tectonics (Hickman, 2004; Hickman and Van Kranendonk, 2004, 2012; Johnson et al., 2017; Smithies et al., 2003; Smithies et al., 2004; Smithies et al., 2009; Smithies et al., 2007b; Van Kranendonk, 2010; Van Kranendonk et al., 2002; Van Kranendonk et al., 2007a; Van Kranendonk et al., 2015).

The EPT is the archetypical granite-greenstone terrane (Kemp et al., 2011). Its dome-like complexes are composed of variably deformed and metamorphosed felsic igneous rocks (granites *sensu lato*) formed through three major magmatic events spanning 300 million years (Hickman and Van Kranendonk, 2004; Van Kranendonk et al., 2004). Over the period 3.53–3.42

Ga, most intrusive rocks were low-K tonalite-trondhjemite-granodiorite (TTG) (Champion and Smithies, 2007; Van Kranendonk et al., 2007b) accompanied by volcanism resulting in the Warrawoona Group (Hickman, 1983). Following a major hiatus in igneous activity (3.42–3.35 Ga) (Hickman, 2008), subsequent magmatic events to 3.22 Ga show a general evolution towards more K_2O–rich granites, reflecting magmatic differentiation and fractionation of the source material (Champion and Smithies, 2007). In almost all cases, these later K-rich magmatic suites were emplaced within the cores of existing TTG-dominated domes (Hickman and Van Kranendonk, 2004). The domes are therefore composite intrusions, comprising successive magmatic episodes spanning up to 300 million years of Earth's early history. Thus, there is the potential to use these crustal remnants to chart the evolution of Palaeoarchaean granitic supersuites through the study of a single dome, with the overarching goal of elucidating early Earth geodynamic processes.

Interpretations of the prevailing nature of early Earth geodynamics, and the generation and stabilization of Earth's first continental crust, tend to fall into two opposing camps: some form of subduction-accretion, in which horizontal forces were dominant (a uniformitarianism approach), versus a setting involving a thick oceanic and/or developing continental plateau that delaminated at its base, and where vertical forces were dominant (Bédard et al., 2003; Johnson et al., 2017; Johnson et al., 2014; Van Kranendonk et al., 2004; Van Kranendonk et al., 2007b). Crustal evolution processes are highly sensitive to the geodynamic setting which drives them (Bédard, 2006; Johnson et al., 2014; Kirkland et al., 2015; Naeraa et al., 2012). Thus, one way to inform the debate on prevailing early Earth

geodynamics is to interrogate Archaean crust with evidence for several magmatic pulses covering the appropriate period of Earth history, such as granitic supersuites within the EPT. We do this, using tools sensitive to inputs into magmatic systems, such as the zircon Lu-Hf and the whole-rock Sm-Nd isotope systems.

The Lu-Hf isotope system has become the tool of choice to understand crustal formation processes through characterization of magmatic sources (Payne et al., 2016; Scherer et al., 2007), given the ability to link a Hf isotopic ratio to a precise date obtained via U-Pb geochronology (Woodhead et al., 2004). Hf isotopes thus provide better fidelity with reference to specific magmatic events that have affected a rock package than whole-rock Sm-Nd isotope data. However, Hf isotopes in zircon have the potential to provide misleading information, specifically with respect to zircons that may represent non-equilibrium phases, and the analysis of metamict and altered zircons. Notwithstanding, the Hf isotope composition of zircon crystals may provide information about the relative contribution and timing of juvenile (mantle-derived) magmatic addition versus reworking (i.e. largely re-melting) of existing crust. As a tool, it is thus highly sensitive to the source(s) of magmatism, and to secular trends discerned through successive magmatic events (Gardiner et al., 2017b). Further, measured Hf isotope ratios allow calculation of Hf model ages that, according to interpretation, may give information about the original age of crust formation – i.e. the timing of original extraction of crustal material from the mantle (Griffin et al., 2002).

Hf isotopes in zircon have been widely deployed to understand crustal processes, in particular the growth of continental crust through time

(Belousova et al., 2010; Dhuime et al., 2012), and they have been used as a tracer for deciphering an evolving geodynamic setting (Kirkland et al., 2015). However, despite the EPT representing one of the few extensively exposed areas of Palaeoarchaean crust on Earth, to date there have been only two Hf isotope studies (Kemp et al., 2015; Nebel et al., 2014), which contain only limited discussion on how the Hf isotope data inform on the magmatic evolution of the Terrane. Composite granite domes, such as those which dominate EPT Palaeoarchaean magmatic rocks, are a unique record of that magmatism, with potential for deciphering the magmatic source. They record successive periods of magmatic events which progressively core the dome, thereby minimizing source heterogeneity, and allow the calculation of some constraints on the input of new (juvenile) material versus reworking of existing crust during magmatism.

In this work, we present and discuss new zircon Hf and whole-rock Nd data from the EPT. These data specifically chart several generations of granitic magmatism that make up one of its major granite complexes, as part of the Mount Edgar Dome. These datasets span the Palaeo- to Mesoarchaean crustal evolution of the dome, which we interrogate to discern secular trends over the time period 3.45–2.83 Ga, a period commonly interpreted as recording a transition from early Earth non-uniformitarian crustal evolution to more modern-style plate tectonic processes (Brown, 2007; Smithies et al., 2004; Smithies et al., 2005, 2007b; Van Kranendonk, 2010; Van Kranendonk et al., 2002; Van Kranendonk et al., 2015). We then use the punctuated magmatic history of the Mount Edgar Dome to constrain the relative addition of juvenile material versus crustal reworking, and frame this

within the competing geodynamic models of early earth crustal accretion. We look at the evidence both for a >3.5 Ga sialic protocrust, and for a change in magmatic style post ca. 3.2 Ga. In this analysis, the data presents insights into the early cratonic growth and stabilization of the EPT during the period 3.53–3.22 Ga.

2. Geological Background

The Pilbara Craton records a geological history stretching from before 3.53 Ga until 2.83 Ga (Hickman, 2012; Hickman and Van Kranendonk, 2012; Van Kranendonk et al., 2007b). The northern part of the Craton is relatively well exposed, while much of the rest, as defined by aeromagnetic and gravity surveys, is unconformably covered by volcanic and sedimentary rocks of the 2.78–2.45 Ga Mount Bruce Supergroup (Hickman and Van Kranendonk, 2012). Extensive mapping by the Geological Survey of Western Australia (GSWA) has indicated that the Pilbara Craton can be subdivided into several terranes (Fig. 1): (a) the 3.53–3.22 Ga East Pilbara Terrane, which preserves evidence of even more ancient Archaean crust (Hickman, 2012; Van Kranendonk et al., 2007a); (b) the 3.28–3.07 Ga West Pilbara Superterrane outcropping in the northwest of the Craton (Hickman, 2016); and (c) the poorly exposed Kurrana Terrane in the southeast, interpreted to include a fragment of the EPT intruded by Mesoarchaean granitic rocks (Hickman, 2012; Hickman, 2016; Hickman and Van Kranendonk, 2012; Van Kranendonk et al., 2006; Van Kranendonk et al., 2007b). All three terranes are unconformably overlain by the clastic sedimentary rocks of the De Grey Superbasin, deposited between 3.06 and 2.93 Ga (Hickman, 2012; Van

Kranendonk et al., 2006). The Pilbara Craton is bordered on its eastern side by the Proterozoic Rudall Province, which reflects juvenile addition into the margin of the Archaean craton (Kirkland et al., 2013). The lithostratigraphy of the EPT is shown in Figure 2.

In common with granite-greenstone terranes in other Archaean cratons of the world, the EPT presents a crustal architecture that has no close analogues in the Phanerozoic, and few in the Proterozoic. Eleven large domal granite complexes are surrounded by greenstone belts, narrow curvilinear belts of steeply-dipping supracrustal successions dominated by metamorphosed volcanic and sedimentary rocks (Fig. 3). Way-up criteria and geochronology reveal that most greenstone belts are broadly synclinal, although their stratigraphic successions are inclined and "young" inwards. However, they differ from most synclines in that the inclination of bedding typically increases inwards, and they are cored by major subvertical faults (Van Kranendonk, 1998). The stratigraphic successions of opposing limbs commonly show major stratigraphic mismatches due to relative vertical displacements of up to 10 km across these axial faults. This feature is attributed to differential vertical uplift of adjacent domes (Hickman, 2012; Hickman and Van Kranendonk, 2004).

The Mount Edgar Dome has a total area of some 4000 km^2, measuring approximately 50 km north–south by 90 km east–west. The dome comprises a central core of 3.48–2.83 Ga granitic rocks assigned to five supersuites - together the Mount Edgar Granitic Complex - overlain and surrounded by the 3.53–2.95 Ga metavolcanic and metasedimentary rocks of the Marble Bar greenstone belt (Fig. 4), part of the Pilbara Supergroup

supercrustal succession. Evidence that these two major units evolved together is provided through both zircon U–Pb geochronology and field relations (Hickman, 2012). The northern and southern boundaries of the Mount Edgar Dome are axial faults separating it from the Muccan and Corunna Downs Domes, respectively, while its western and eastern contacts, concealed by the 2.78–2.63 Ga Fortescue Basin, are also interpreted to be faulted contacts with the North Pole, Warrawagine, Yilgalong, and McPhee Domes (Fig. 3).

2.1. Granite Suites of the Mount Edgar Dome

The Mount Edgar Granitic Complex grew by the episodic emplacement of granitic intrusions, within which distinct compositional and textural plutonic phases have been identified. Concurrently, the overlying ca. 15 km-thick greenstone succession (the Pilbara Supergroup; Fig. 2) accumulated during eight successive volcanic cycles (Hickman, 2012; Van Kranendonk et al., 2007a; Van Kranendonk et al., 2007b). Across the EPT, four granitic supersuites (namely the Callina, Tambina, Emu Pool, and Cleland) are known to have intruded during its Palaeoarchaean evolution, and a 3.53–3.49 Ga granitic supersuite, yet to be identified in outcrop, can be inferred through xenocrystic zircons (Gardiner et al., 2017a; Hickman, 2016). Additionally, four Mesoarchaean supersuites intruded between 3.20–2.83 Ga. Five of these supersuites have been identified in the Mount Edgar Dome (Fig. 4), and thus the dome's known magmatic history stretches from ca. 3.48 to 2.83 Ga.

The voluminous Tambina Supersuite (3.451–3.416 Ga) is particularly well exposed along the southern and western parts of the Mount

Edgar Dome (Fig. 4), and is predominantly sodic in composition, including both tonalite and granodiorite phases (Champion and Smithies, 2007; Van Kranendonk et al., 2006). The Tambina Supersuite was emplaced at mid-crustal levels and subsequently buried to depths up to 25 km, accompanied by metamorphism to upper amphibolite facies (Collins and Van Kranendonk, 1999). The Fig Tree Gneiss, a component of the Tambina Supersuite, crops out only within the core of the Mount Edgar Dome, and is everywhere compositionally banded and strongly deformed (Collins, 1989; Kloppenburg, 2003).

The Emu Pool Supersuite comprises widespread 3.32–3.27 Ga intrusions of monzogranite and granodiorite, and ranges in composition from trondhjemite to syenogranite (Van Kranendonk et al., 2006). All intrusions of the Emu Pool Supersuite are only moderately to weakly foliated. Subsequently, the entire EPT was affected by the Cleland Supersuite magmatic event (Barley and Pickard, 1999). The intrusive rocks of the Cleland Supersuite (3.27–3.22 Ga) are dominantly monzogranite, and crop out in most domes of the EPT.

The Mesoarchaean 2.85–2.83 Ga Split Rock Supersuite comprises highly fractionated, post-tectonic Sn–Ta–Li–Be-bearing monzogranite to syenogranite plutons and pegmatites, which were emplaced into the East Pilbara and Kurrana Terranes. Associated ore minerals, cassiterite and tantalite, have been directly dated through U-Pb SIMS to 2.88–2.84 Ga (Kinny, 2000). This suite forms a northwest–southeast trending belt of intrusions orthogonal to the northern, tectonized boundary of the Mosquito Creek Basin. This geometry could suggest emplacement along a failed rift

that developed towards the end of the ca. 2.90 Ga Mosquito Creek Orogeny (Van Kranendonk et al., 2006) or, alternatively, might trace the drift of the Pilbara Craton across a ca. 2.85 Ga hot spot (Hickman, 2016).

3. Sampling and Results

3.1. Samples and Results

Published geochronology from across the EPT has included zircon U-Pb ages from 220 felsic igneous rocks representing all domes and greenstone belts, and from age groupings of numerous detrital zircons in many sandstone samples (Hickman, 2016; Nelson, 1999b). This dataset established that both felsic and mafic magmatism occurred within discrete events (Champion and Smithies, 2007; Hickman, 2012; Hickman and Van Kranendonk, 2004, 2012; Van Kranendonk et al., 2002; Van Kranendonk et al., 2006; Van Kranendonk et al., 2007b). Samples used in this study came from four of the five Mount Edgar Granite Complex supersuites identified on the basis of U-Pb zircon ages. These supersuites (Tambina, Emu Pool, Cleland and Split Rock) define four major magmatic events, at: 3451–3416; 3324–3277; 3274–3223; and 2851–2831 Ma, respectively.

A total of 27 samples from the Mount Edgar Dome were analyzed for zircon Lu-Hf isotopes using LA-MC-ICP-MS. Additionally, four samples from the Mount Edgar Dome, and one sample from each of the Muccan and Shaw Domes, were analyzed for whole-rock Sm-Nd isotopes (analytical methodologies in Appendix A). Mount Edgar sample localities are shown in Figure 5, and a summary of sample localities, descriptions and results in Table 1. All Hf isotope analyses were performed on zircon grains

previously dated by SHRIMP U-Pb geochronology (references in Supplementary Data), providing the magmatic ages for interpretation of both the zircon Hf, and whole-rock Sm-Nd, isotope analysis. Full analytical results are presented in Table 2 (zircon Hf isotope data) and Table 3 (whole-rock Nd isotope data).

Hf isotope evolution plots showing the distribution of calculated initial $^{176}Hf/^{177}Hf$ values, presented in epsilon units (εHf) versus magmatic age, are detailed in Fig. 6. Analyses interpreted as inherited, distinguished on the basis of U-Pb geochronology, are identified in the evolution plots. The four new Mount Edgar Dome whole-rock Sm-Nd data from the Tambina, Emu Pool and Split Rock supersuites are shown on a εNd evolution plot in Fig. 7. Appendix B contains a detailed discussion of the Hf and Nd isotope data of each supersuite.

4. Discussion

4.1. Hf isotopic maps

Isotope maps provide a useful way of spatially visualizing isotopic trends, potentially allowing identification of discrete crustal blocks and their bounding faults, with potential for mineralization (Champion and Huston, 2016; Mole et al., 2014; Tomlinson et al., 2004). Time-slicing the isotope data and producing time-bracketed maps permits the temporal interpretation of spatial isotope data. Time-slicing also resolves inherited information within the same broad geographic domain.

Figure 8 shows an εHf isotopic map of Mount Edgar delineated by geological boundaries, where the supersuites are coloured for median εHf,

A trend from more evolved values (negative εHf) towards more juvenile (i.e. more radiogenic, positive εHf) is observed from the core to the rim of the dome. Allied with the existing zircon U-Pb age data that show the granite dome to be cored by younger magmatic suites, these data suggest that the younger units intruding into the core of the dome become progressively more isotopically evolved (i.e. the granitic melts are progressively sourcing more evolved crust towards the centre of the dome).

4.2. A Note On $^{176}Lu/^{177}Hf$ ratios

Interpretations of Hf isotope arrays through time, and calculation of two-stage Hf model ages, generally use an isotopic evolution trajectory defined by a fixed $^{176}Lu/^{177}Hf$ ratio of a source. Such an evolution line is taken to represent the isotopic trajectory along which successive daughter products of crustal reworking lie. Data that deviate from this line are interpreted to show the addition of either juvenile, or more evolved non-cognate material. Studies typically use a $^{176}Lu/^{177}Hf$ ratio of 0.015, the isotopic composition of modern andesitic crust (Griffin et al., 2002). However, this ratio is perhaps inappropriate for modelling Archaean crustal evolution where TTGs and their derivatives dominate. Thus, for early Earth studies, a $^{176}Lu/^{177}Hf$ ratio of 0.010 may be more suitable (e.g., Kröner et al. (2012)), and this ratio is employed for the Hf evolution trend in Fig. 6.

4.3. Model Ages

Remnants of crust older than the Pilbara Supergroup are known to crop out in only two areas of the EPT (McNaughton et al., 1988; Nelson, 1999a, b). Two-stage Hf model ages (T_{DM}^2) were resolved in this work using

$^{176}Lu/^{177}Hf$ ratios of both 0.010 and of 0.015 for the reasons given above. For a $^{176}Lu/^{177}Hf$ ratio of 0.010, all Mount Edgar samples with a magmatic age > 3.2 Ga resolve to Eoarchaean model ages, with a median age of ca. 3.60 ± 0.1 Ga (1σ). Using a $^{176}Lu/^{177}Hf$ ratio of 0.015, the same samples resolve to model ages with a median of 3.67 ± 0.1 (1σ).

There are a number of assumptions in both the calculation and application of Hf model ages, specifically: (a) that the magma source reflects a single component rather than a mixture of source components with different initial fractionation events; (b) the $^{176}Lu/^{177}Hf$ ratio employed is appropriate for the reservoir prior to zircon crystallization; and (c) the model used to define depleted mantle (DM) accurately tracks the secular change in mantle composition. Nonetheless, given average evolutionary trends, all the EPT samples here resolve to model ages < 4.0 Ga regardless of which $^{176}Lu/^{177}Hf$ ratio is used for their calculation.

In hunting for evidence of crust of Hadean age, Kemp et al. (2015) reported LA-MC-ICP-MS Hf isotope analysis from previously dated GSWA zircon mounts from 12 samples of sandstones (i.e. detrital zircons), and from two samples from magmatic rocks, targeting domains interpreted to represent grains inherited from an earlier magmatic episode. The magmatic rocks sampled were the ca. 3.66 Ga gneissic enclave in the Tambina Supersuite from the Warrawagine Dome, and a ca. 3.2 Ga monzogranite from the Cleland Supersuite, Muccan Done. The zircons in all reported samples (detrital and magmatic) have U-Pb crystallization ages of 3.80–3.55 Ga. The bulk of the dataset yield εHf of ca. 0.0, with three older (> 3.68 Ga) zircon grains having more evolved Hf signatures (εHf -2 to -3). Two-stage Hf model

ages calculated using the conventional depleted mantle model would resolve to ca. 3.9–4.0 Ga. If a chondritic mantle model is assumed (e.g., Caro and Bourdon (2010)), then all these zircon grains, except the three anomalously old zircons, yield two-stage Hf model ages of 3.7–3.6 Ga, suggesting an Eoarchaean age of original crust extraction from the mantle.

The four new whole-rock Sm-Nd isotope analyses from the magmatic rocks of the Mount Edgar Granitic Complex reported here have two-stage Nd model ages of between 3.65–3.59 Ga (Table 3). These ages are in accord with previous whole-rock Sm-Nd isotope analysis from the felsic volcanic rocks surrounding the Mount Edgar Dome; the ca. 3.47 Ga Duffer Formation volcanics yield two-stage Nd model ages of 3.62–3.52 Ga (Smithies et al., 2007a).

4.4. Early Archaean Evolution (3.6–3.2 Ga)

The timing of the onset of “modern” plate tectonics, defined by deep, steep subduction of oceanic lithosphere, is controversial (Condie and Pease, 2008). Many workers are of the opinion that the Pilbara Craton experienced a fundamental shift in tectonic style from an early (> 3.2 Ga) period of plume-related magmatism, to a later period (< 3.2 Ga) when the prevailing geodynamic processes were more akin to today, i.e. mobile lid tectonics with steep subduction (Hickman, 2004; Kemp et al., 2011; Smithies et al., 2003; Smithies et al., 2004; Smithies et al., 2007b; Van Kranendonk et al., 2002; Van Kranendonk et al., 2010; Van Kranendonk et al., 2015). It is thus helpful to consider the Mount Edgar isotope data in terms of the rocks’ petrogenesis falling under two potentially different geodynamic regimes: (i) early Archaean, pre-3.2 Ga magmatism (i.e. the Tambina, Emu Pool and

Cleland supersuites), and (ii) those with magmatic crystallization ages of Mesoarchaean onwards (considered here, the Split Rock Supersuite).

The period 3.6–3.2 Ga is arguably key with respect to Archaean cratonic stabilization and growth, since this represents some of the earliest recorded magmatism, that globally is predominantly comprised of 'grey gneisses', dominated by TTG suites (Moyen, 2011). In the main, the Hf isotopes from the oldest of the Mount Edgar Dome supersuites discussed here, the Tambina Supersuite, yield relatively juvenile εHf (i.e. radiogenic Hf values close to DM), ranging from +4 to -2. Most workers have interpreted that the TTG magmas for the Tambina Supersuite were derived by partial melting of older crust, either the TTG rocks of the Callina Supersuite (Pawley et al., 2004), or, more generally, infracrustal melting of enriched hydrated basaltic crust (Champion and Smithies, 2007; Smithies et al., 2009; Van Kranendonk et al., 2015). Through the younger Palaeoarchaean supersuites (Emu Pool and Cleland), a general secular trend towards more evolved values (negative εHf) is observed (Fig. 6A). The implication of this trend is that the later Palaeoarchaean supersuites were derived in large part from partial melting of older TTG granitic crust.

Champion and Smithies (2007) noted a correlation between whole-rock Nd isotope data (expressed as εNd), and bulk-rock chemistry, specifically K_2O and Th, for high-Al, sodic ca. 3.3 Ga graniotoids (their definition). In order to explore this relationship further, we plot εHf versus K_2O for the Palaeoarchaean supersuites (Fig. 9). All plotted samples of the Emu Pool supersuite have Al_2O_3 > 14 wt%, and thus fall into the "high Al" definition of Champion and Smithies (2007). We find no discernable correlation

between εHf and K_2O within individual supersuites. However, the youngest Palaeoarchaean supersuite plotted, Cleland, has notably higher whole-rock K_2O with an εHf signal more evolved than the other two supersuites, consistent with crustal reworking and differentiation towards more K-rich granitoids.

The Hf data discussed here are taken from supersuites of a single granite dome. This geographic focus arguably minimizes lateral source heterogeneity, important when constraining the evolution of supersuites comprising a number of individual units. However, it should be recognized that other domes of the EPT contain somewhat different supersuite assemblages to that of the Mount Edgar Dome (Van Kranendonk et al., 2006), and also developed at different rates (Hickman and Van Kranendonk, 2004). Thus, while the crustal evolution of the Mount Edgar Dome may be typical of the EPT, it is not representative of Mesoarchaean granites in the Pilbara Craton.

4.4.1. Estimation of Juvenile Input in >3.2 Ga Mount Edgar Magmatism

A first-order quantitative estimate on the required input of juvenile (depleted mantle) material during crustal reworking is helpful when considering likely geodynamic settings driving that magmatism. To achieve this, a framework for modelling was constructed within initial $^{176}Hf/^{177}Hf$ space by calculating points representing the median age and median initial $^{176}Hf/^{177}Hf$ ratio of the three >3.2 Ga supersuites (Fig. 10). These are labelled magmatic events M1–M3: Early TTG M1 (Tambina; 3442 Ma, $^{176}Hf/^{177}Hf$ = 0.280596); M2 (Emu Pool; 3308 Ma, $^{176}Hf/^{177}Hf$ = 0.280661); and M3 (Cleland; 3235 Ma, $^{176}Hf/^{177}Hf$ = 0.280646). Evolution lines defined by source $^{176}Lu/^{177}Hf$ values of both 0.010 and 0.015, are plotted from M1. These

represent isotope arrays along which the M1 crustal packet may evolve. The 0.010 line (in green) intersects the 3308 Ma M2 event at a less radiogenic Hf value than that of M2 ($^{176}Hf/^{177}Hf$ = 0.280620; E2). This model suggests that the Hf composition of M2 cannot be attained solely through reworking of the M1 TTG crust, otherwise M2 would lie on the evolution line. Thus, an input of material with a more radiogenic, i.e. more juvenile, Hf isotopic signature is required to produce a melt with the median Hf isotope composition of M2.

A simple quantification of this putative 3308 Ma juvenile input to yield M2 can be estimated through a linear mass balance calculation between the evolved Hf isotope end-member composition (E2 in Fig. 10), and a nominated juvenile source, J2, assumed to be an input of mafic melt. J2 is likely related to the mafic volcanic cycle, which is here taken as having the Hf isotope composition of DM at 3308 Ma (J2: $^{176}Hf/^{177}Hf$ = 0.280807). Thus, an implicit assumption here is made that the modelled depleted mantle in the early Archaean is consistent with the modern Earth definition (e.g., that of Griffin et al. (2000)), and that we are not following a chondritic model for this period of Earths history. This mass balance, an approximation due to the different ratios of ^{176}Lu to ^{177}Hf in the mantle reservoir versus that of M1, implies that a juvenile input of some 22% by mass is required, i.e. approximately one fifth of input into the magmatic system, to give rise to M2 crust, with the remainder being sourced from M1 TTG crust. A similar calculation using a source $^{176}Lu/^{177}Hf$ value of 0.015 gives a juvenile input of ca. 15%. Extending this approach to M3, and extrapolating the Hf evolution line from M1 to E3, suggests that the M3 Hf isotope composition requires only

minimal (5%) juvenile input of a J3 DM source. The implications for these figures are discussed below.

4.4.2. Implications for Early Earth Crustal Processes

The secular pattern of Hf isotopes during the early evolution of an Archaean terrane may help inform the debate regarding the development and stabilization of its cratonic core. Specifically, the pattern may help distinguish between two end-member geodynamic models for the Palaeoarchaean EPT: a uniformitarian scenario, dominated by horizontal forces (Barley, 1993; Bickle et al., 1980; Krapez, 1993; Krapez and Eisenlohr, 1998), and another where Earth's early crust evolved by non-uniformitarian processes, possibly plume-driven, and dominated by vertical forces (Collins et al., 1998; François et al., 2014; Hickman, 1981, 1983, 1984; Hickman, 2012; Johnson et al., 2017; Johnson et al., 2014; Thébaud and Rey, 2013; Van Kranendonk, 2010; Van Kranendonk et al., 2014; Van Kranendonk et al., 2007b; Williams and Collins, 1990). This latter non-uniformitarian model differs significantly from the plate tectonic paradigm, in that crust grew through differentiation within a delaminating volcanic-plateau, reflecting the elevated mantle temperature at that time (Bédard, 2006; Hickman and Van Kranendonk, 2004, 2012; Johnson et al., 2014; Kamber, 2015; Smithies et al., 2009; Van Kranendonk et al., 2007a).

In the volcanic plateau model, the developing Palaeoarchaean crust acts as a thickening "stagnant lid" that supports partial convective overturn driven by differential buoyancy - so-called sagduction (Johnson et al., 2016) - which has been interpreted as giving rise to the classic dome-and-keel architecture observed within the EPT (e.g., Van Kranendonk et al. (2014)). In

the case of the EPT, the volcanic plateau model has been extended by the suggestion of the existence of older underlying continental crust, i.e. a sialic protocrust, onto which the early volcanics were extruded, and within which early magmatism developed (Hickman, 1981). The existence of this hypothetical older underlying felsic crust (Hickman, 2012; Van Kranendonk et al., 2007a) is supported by several lines of evidence, notably (a) lateral continuity of greenstone belts across the EPT; (b) the existence of identifiable unconformities between greenstone successions; and (c) structural evidence implying interleaved felsic units found within the greenstone belts were contemporaneous with intrusive magmatic supersuites.

Several further lines of evidence are invoked to differentiate between the plate tectonic and volcanic plateau models. One of the stronger arguments is the distinct suite of TTG suites, and their K-rich granitic derivatives, which constitute the bulk of felsic magmatism in the EPT as well as in the exposed deeper levels of Archaean continental crust worldwide. Such rocks are high in SiO_2, Al_2O_3 and Na_2O, with a high Sr/Y ratio (Moyen and Martin, 2012). The contemporaneous genesis of both high- and low-P TTGs from 3.5 to 3.2 Ga has been observed in the EPT, reflected by the presence of both high-Al and low-Al rocks of similar magmatic ages (Champion and Smithies, 2007). This evidence has been interpreted as supporting a non-subduction origin, since such simultaneous magma formation of disparate suites has been proposed to be possible only through infracrustal melting of mafic rocks near the base of > 50 km-thick crust (Moyen et al., 2007; Van Kranendonk et al., 2014).

A fundamental tenet in using Hf and Nd isotopes to develop geodynamic models, as attempted here for the Mount Edgar Dome, is whether the data trends through time represent dominantly new crust addition, or dominantly reworking of older crustal material. In this context, whether the genesis of EPT Palaeoarchaean supersuites can be explained through a dominance of reworking of existing crust, with only minor input of new juvenile material, or whether there is a requirement for an extensive input of new juvenile addition.

Taking a modern analogue, a long-lived subduction system, such as the Circum-Pacific accretionary margin, shows consistent trends in Hf isotopes towards more radiogenic values over extended periods of time (Collins et al., 2011). Modern orogenic systems may present an evolution in the overall Hf and Nd isotope signature towards more evolved values (less radiogenic) with successive magmatic events, but this trend is often reflective of a change in orogenic style towards continent–continent collision and thus enhanced reworking of existing crust (Gardiner et al., 2016; Roberts, 2012).

Our modelling, albeit a simplistic first-order approach, estimates that a ca. 20% input of juvenile material was required to account for the genesis of the Emu Pool Supersuite. In terms of mass balance, an average juvenile input of 20% into the Emu Pool magmatic system, is clearly not adequate enough to move the median Hf isotope data towards a sufficiently juvenile Hf signal, such as those observed in modern subduction analogues.

The younger Palaeoarchaean supersuites (Emu Pool and Cleland) have been interpreted to have been largely derived from the melting of older granitic crust, on the basis of both geochemical and previous Nd

isotopic evidence (Barley and Pickard, 1999; Champion, 2013; Smithies et al., 2003). This model of extensive crustal reworking of earlier TTG suites is supported by the new Mount Edgar Hf data arrays, which trend towards evolved, i.e. sub-chondritic, εHf values. Further, all three Palaeoarchaean supersuites resolve to consistent Eoarchaean model ages, implying a common original source reservoir. Such an interpretation is also supported by the new Nd data, which for Mount Edgar also exhibit a shift towards more evolved εNd values with time, from the Tambina (average +0.2) to the Emu Pool (-1.4).

4.4.3. Eoarchaean Sialic Protocrust?

The possible existence of a cryptic > 3.53 Ga sialic protocrust underlying the EPT, onto which the earliest komatiitic and basaltic volcanics were erupted, and within which the earliest TTGs developed, has been proposed (e.g., Hickman (2012)). A number of lines of evidence from previous work in the EPT lend support to the existence of some sort of protocrust; (a) enclaves of anorthositic gabbro (3.58 Ga; McNaughton et al. (1988)), and trondhjemite gneiss (3.65 Ga; Nelson (1999b), Williams (2000)), found within the granites; (b) rare xenocrystic zircons recording U-Pb SIMS ages of 3.72 Ga (Thorpe et al., 1992b); (c) common detrital zircons with magmatic crystallization ages between 3.8 and 3.53 Ga found in 3.46–2.93 Ga metasedimentary rocks from the Pilbara region (Bagas et al., 2008; Bagas et al., 2005; Hickman, 2012; Kemp et al., 2015; Van Kranendonk et al., 2002; Van Kranendonk et al., 2006; Van Kranendonk et al., 2007b); (d) Nd model ages of between 3.71 and 3.56 Ga (Gruau et al., 1987; Hamilton et al., 1981; Hickman, 2012; Jahn et al., 1981; Smithies et al., 2007a; Van Kranendonk et

al., 2007b), augmented by the new Sm–Nd data reported here; (e) evolved εNd (-3.3) from the Dresser Formation suggesting incorporation of an older component (Tessalina et al., 2010); (f) anomalously high $^{238}U/^{204}Pb$ from the Dresser Formation suggestive of the derivation of Pb from a highly enriched felsic crust ca. 3.7 Ga (Thorpe et al., 1992a).

The Hf isotope data presented here hint at such a protocrust. The Cleland Supersuite at ca. 3.45 Ga shows a spread of values towards more evolved εHf, implying some input of recycled earlier crust; the mean Hf two-stage model ages of all three > 3.2 Ga supersuites resolve to 3.7–3.6 Ga. Both of these lines of evidence are consistent with the previous work as outlined above, and suggest the existence of some form of pre-3.5 Ga protocrust, at least to the late Eoarchaean. However, the nature of such a protocrust, and the volume of felsic material contained therein, cannot be constrained through the Hf isotope data.

4.5. A change in magmatic style into the Mesoarchaean?

During the Mesoarchaean, the EPT was intruded by several granitic supersuites (Sisters, Elizabeth Hill and Mount Billroth) some 400 MYr prior to the genesis of the Split Rock Supersuite. Such Mesoarchaean crust is widespread in the northwest Pilbara (Hickman, 2012; Hickman, 2016; Smithies, 2000; Smithies et al., 2004; Smithies et al., 2007a; Van Kranendonk et al., 2010; Van Kranendonk et al., 2007b), and may have been a source for magmatism during the 2.95–2.92 Ga North Pilbara Orogeny (Hickman, 2016; Smithies et al., 2004; Smithies et al., 2007a).

Mesoarchaean rocks of the West Pilbara Superterrane provide evidence, in the form of lithological, geochemical and structural differences,

that argue for a shift in tectonic style between the Palaeoarchaean formation of the EPT and the Mesoarchaean formation of the West Pilbara Superterrane (Hickman, 2004, 2016; Smith et al., 1998; Smithies et al., 2005, 2007b; Van Kranendonk et al., 2010). Whole-rock major geochemical trends from across the EPT show an increase in K_2O and K_2O/Na_2O with decreasing magmatic age from Palaeo-Mesoarchaean granites (Fig. 11). These trends may be due to increasing differentiation of the crust through reworking.

The Sm-Nd isotope data for the entire Pilbara Craton, while incomplete in terms of coverage, may be similarly interpreted. Figure 12 presents Sm-Nd isotope maps for the Pilbara Craton, presented as two-stage Nd model age (T_{DM}^2). The model age data is plotted both for all Pilbara samples (Fig. 12A), and for felsic samples only (Fig. 12B). Further, the model age data for the felsic samples only, is further subdivided into that screened for Palaeoarchaean (principally the EPT) magmatic ages, and that screened for Mesoarchaean (West Pilbara Superterrane) magmatic ages (Figs. 12C and D respectively).

Inspection shows that the EPT data record older Nd model ages. This is in striking contrast with the data from the West Pilbara Superterrane that yields younger Nd model ages, consistent with its Mesoarchaean magmatic suites having developed within a plate tectonic regime during spreading and convergence. Notably, there are no clear differences between the Nd model age map drawn using all the Pilbara Nd data, and that only for the felsic units, which may indicate the mafic units are assimilating crust, providing support for an older basement underlying the EPT.

Comparison of the two time slices (Fig. 12C and D) show an inverse relationship. The EPT exhibits significant magmatism with Nd model ages > 3.5 Ga (Fig. 12C). By contrast magmatism in the West Pilbara Superterrane is dominated by that with significantly younger Nd model ages (Fig. 12D). Such patterns in isotopic values interpreted through model ages, could be interpreted to reflect the process of cratonization, in which crust becomes stabilized and able to support marginal subduction leading to production of new crust after 3.2 Ga.

Nd isotopic maps for the Pilbara Craton have been presented before (e.g., Champion and Huston (2016)). These workers interpreted the consistently older EPT Nd model ages (compared to the West Pilbara Superterrane) as reflecting the reworking of older EPT basement through younger (2.9–2.8 Ga) supersuites, and that the jump in model ages across the EPT-West Pilbara Superterrane boundary may reflect magmatism in the latter terrane reworking younger underlying basement.

The Hf isotope data from the 2.8 Ga Split Rock Supersuite reported here yields εNd of -7.1 (Fig. 7), and a mean εHf of -4.6, somewhat more evolved than those data reported for the Palaeoarchaean supersuites. These Mesoarchaean data lie above the Hf evolution line (Fig. 6), necessitating an input of additional juvenile material into the magmatic system, in addition to reworking of the existing, older > 3.2 Ga crust. This more evolved Hf isotope signature may be consistent with the Mesoarchaean supersuites reflecting a switch from dominantly Na-rich TTG type rocks to more K-rich granites. Such a switch is seen in the Pilbara granite whole-rock geochemistry compilation (Fig. 11). However, an alternate explanation may be

that the Split Rock Supersuite was largely derived from the partial melting of a different crustal source mixture than the > 3.2 Ga EPT granites, which included ca. 3.2 Ga juvenile crust that post-dated the earlier development of the EPT. The Split Rock Hf data are scattered, however Mesoarchaean Nd data for the Split Rock Supersuite from across the EPT also show significant variability (Smithies et al., 2007a).

5. Conclusions

New zircon Hf and whole-rock Nd isotope data from the Mount Edgar Dome, East Pilbara Terrane, suggest Palaeoarchaean magmatic processes that involved a dominance of reworking of existing crust over significant new juvenile material. These data together support a geodynamic model that allows for major reworking of existing crust, requiring only a minor input of juvenile material from 3.5–3.2 Ga. That is, one which accommodates the successive re-melting of existing crust during epochs of magmatism, rather than continuous magmatic activity with a dominance of juvenile input. The minor contribution of juvenile material may be accounted for by the fact that some input of mafic material is likely, either as entrained mafic source material, or via incorporation of sinking greenstones during the doming events (Johnson et al., 2016).

This dominance of crustal reworking over the growth of new juvenile crust with successive magmatism is consistent with other lines of evidence, both geochemical and isotopic (Barley and Pickard, 1999; Champion, 2013; Smithies et al., 2003), for secular change. Here, we interpret the new data as supporting a volcanic plateau model as the dominant > 3.2

Ga geodynamic setting of the East Pilbara Terrane, one which was dominated by vertical rather than horizontal tectonics. The Hf and Nd model ages are aligned with other lines of evidence that suggest some sort of pre-3.5 Ga protocrust, albeit of unknown extent. This study has not revealed any evidence for early Eoarchaean or Hadean crust.

Acknowledgements

NJG acknowledges Curtin University for financial support. AHH and YL publish with permission of the Executive Director, Geological Survey of Western Australia. Hugh Smithies and Simon Wilde are thanked for comments on a draft of this manuscript. We thank David Champion and Kristoffer Szilas for constructive reviews, and Randall Parrish for efficient editorial handling.

References

Arndt, N., Bruzak, G., Reischmann, T., 2001. The oldest continental and oceanic plateaus: geochemistry of basalts and komatiites of the Pilbara Craton, Australia. Geological Society of America Special Paper 351, 359-387.

Bagas, L., Bierlein, F.P., Bodorkos, S., Nelson, D.R., 2008. Tectonic setting, evolution and orogenic gold potential of the late Mesoarchaean Mosquito Creek Basin, North Pilbara Craton, Western Australia. Precambrian Research 160, 227-244.

Bagas, L., Farrell, T.R., Nelson, D.R., 2005. The age and provenance of the Mosquito Creek Formation, Annual Review. Geological Survey of Western Australia, pp. 62-70.

Barley, M.E., 1993. Volcanic, sedimentary and tectonostratigraphic environments of the ~ 3.46 Ga Warrawoona Megasequence: a review. Precambrian Research 60, 47-67.

Barley, M.E., Loader, S.E., McNaughton, N.J., 1998. 3430 to 3417 Ma calc-alkaine volcanism in the McPhee Dome and Kelly Belt, and growth of the eastern Pilbara Craton. Precambrian Research 88, 3-23.

Barley, M.E., Pickard, A.L., 1999. An extensive, crustally-derived, 3325 to 3310 Ma silicic volcanoplutonic suite in the eastern Pilbara Craton: evidence

from the Kelly Belt, McPhee Dome and Corunna Downs Batholith. Precambrian Research 96, 41-62.
Bédard, J.H., 2006. A catalytic delamination-driven model for coupled genesis of Archaean crust and sub-continental lithospheric mantle. Geochimica et Cosmochimica Acta 70, 1188-1214.
Bédard, J.H., Brouillette, P., Madore, L., Berclaz, A., 2003. Archaean cratonization and deformation in the northern Superior Province, Canada: an evaluation of plate tectonic versus vertical tectonic models. Precambrian Research 127, 61-87.
Belousova, E.A., Kostitsyn, Y.A., Griffin, W.L., Begg, G.C., O'Reilly, S.Y., Pearson, N.J., 2010. The growth of the continental crust: Constraints from zircon Hf-isotope data. Lithos 119, 457-466.
Bickle, M.J., Bettenay, L.F., Boulter, C.A., Groves, D.I., Morant, P., 1980. Horizontal tectonic interaction of an Archean gneiss belt and greenstones, Pilbara Block, Western Australia. Geology 8, 525-529.
Blichert-Toft, J., Albarède, F., 1997. The Lu-Hf isotope geochemistry of chondrites and the evolution of the mantle-crust system. Earth and Planetary Science Letters 148, 243-258.
Brown, M., 2007. Metamorphic Conditions in Orogenic Belts: A Record of Secular Change. International Geology Review 49, 193-234.
Caro, G., Bourdon, B., 2010. Non-chondritic Sm/Nd ratio in the terrestrial planets: Consequences for the geochemical evolution of the mantle–crust system. Geochimica et Cosmochimica Acta 74, 3333-3349.
Champion, D.C., 2013. Neodynium depleted mantle model age map of Australia. Geoscience Australia, Canberra.
Champion, D.C., Huston, D.L., 2016. Radiogenic isotopes, ore deposits and metallogenic terranes: Novel approaches based on regional isotopic maps and the mineral systems concept. Ore Geology Reviews 76, 229-256.
Champion, D.C., Smithies, R.H., 2007. Chapter 4.3 Geochemistry of Paleoarchean Granites of the East Pilbara Terrane, Pilbara Craton, Western Australia: Implications for Early Archean Crustal Growth. 15, 369-409.
Cloud, P., 1988. Oasis in Space, Earth History from the Beginning. WW Norton and Company, New York.
Collins, W.J., 1989. Polydiapirism of the Archean Mount Edgar Batholith, Pilbara Block, Western Australia. Precambrian Research 43, 41-62.
Collins, W.J., Belousova, E.A., Kemp, A.I.S., Murphy, J.B., 2011. Two contrasting Phanerozoic orogenic systems revealed by hafnium isotope data. Nature Geoscience 4, 333-337.
Collins, W.J., Van Kranendonk, M.J., 1999. Model for the development of kyanite during partial convective overturn of Archean granite–greenstone terranes: the Pilbara Craton, Australia. Journal of Metamorphic Geology 17, 145-156.
Collins, W.J., Van Kranendonk, M.J., Teyssier, C., 1998. Partial convective overturn of Archaean crust in the east Pilbara Craton, Western Australia: driving mechanisms and tectonic implications. Journal of Structural Geology 20, 1405-1424.
Condie, K.C., Pease, V., 2008. When Did Plate Tectonics Begin on Planet Earth?

Dhuime, B., Hawkesworth, C., Cawood, P.A., Storey, C.D., 2012. A Change in the Geodynamics of Continental Growth 3 Billion Years Ago. Science 335, 1334-1336.
François, C., Philippot, P., Rey, P., Rubatto, D., 2014. Burial and exhumation during Archean sagduction in the East Pilbara Granite-Greenstone Terrane. Earth and Planetary Science Letters 396, 235-251.
Gardiner, N.J., Hickman, A.H., Kirkland, C.L., Lu, Y.J., Johnson, T.E., Wingate, M.T.D., 2017a. New Hf Isotopic Insights into the Paleoarchean Magmatic Evolution of the Mount Edgar Dome, Pilbara Craton: Implications for Early Earth and Crust Formation Processes. Geological Survey of Western Australia.
Gardiner, N.J., Kirkland, C.L., Johnson, T.E., Smithies, R.H., 2017b. Crustal Melting Controls on Lu-Hf Isotope Systematics. Geochemical Perspectives Letters in review.
Gardiner, N.J., Kirkland, C.L., Van Kranendonk, M.J., 2016. The Juvenile Hafnium Isotope Signal as a Record of Supercontinent Cycles. Scientific Reports 6, 38503.
Griffin, W., Pearson, N.J., Belousova, E., Jackson, S.E., van Achterbergh, E., O'Reilly, S.Y., Shee, S.R., 2000. The Hf isotope composition of cratonic mantle: LAM-MC-ICPMS analysis of zircon megacrysts in kimberlites. Geochimica et Cosmochimica Acta 64, 133-147.
Griffin, W., Pearson, N.J., Belousova, E., Saeed, A., 2007. Reply to 'Comment to short-communication: Hf-isotope heterogeneity in zircon 91500' by W.L. Griffin, N.J. Pearson, E.A. Belousova, A. Saeed (Chemical Geology 233 (2006) p. 358-363)' by F. Corfu. Chemical Geology 244, 354-356.
Griffin, W.L., Wang, X., Jackson, S.E., Pearson, N.J., O'Reilly, S.Y., Xu, X., Zhou, X., 2002. Zircon chemistry and magma mixing, SE China: In-situ analysis of Hf isotopes, Tonglu and Pingtan igneous complexes. Lithos 61, 237-269.
Gruau, G., Jahn, B.-m., Glikson, A.Y., Davy, R., Hickman, A.H., Chauvel, C., 1987. Age of the Archean Talga-Talga Subgroup, Pilbara Block, Western Australia, and early evolution of the mantle: new Sm-Nd isotopic evidence. Earth and Planetary Science Letters 85, 105-116.
Hamilton, P., Evensen, R., O'Nions, R.K., Glikson, A.Y., Hickman, A.H., 1981. Sm-Nd dating of the North Star basalt, Warrawoona Group, Pilbara Block, Western Australia, in: Glover, J.E., Groves, D.I. (Eds.), Archaean Geology, pp. 187-192.
Hawkesworth, C.J., Kemp, A.I.S., 2006. Using hafnium and oxygen isotopes in zircons to unravel the record of crustal evolution. Chemical Geology 226, 144-162.
Hickman, A.H., 1981. Crustal evolution of the Pilbara Block, in: Groves, D.I. (Ed.), Archaean Geology, Second International Archaean Symposium, Perth, pp. 57-69.
Hickman, A.H., 1983. Geology of the Pilbara Block and its environs. Bulletin of the Geological Survey of Western Australia 127, 268.
Hickman, A.H., 1984. Archaean diapirism in the Pilbara Block, Western Australia, in: Kröner, A., Greiling, R. (Eds.), Precambrian Tectonics Illustrated. E. Schweizerbarts'che Verlagsbuchhlung, Stuttgart, pp. 113-127.

Hickman, A.H., 2004. Two contrasting granite–greenstone terranes in the Pilbara Craton, Australia: evidence for vertical and horizontal tectonic regimes prior to 2900Ma. Precambrian Research 131, 153-172.
Hickman, A.H., 2008. Regional review of the 3426–3350 Ma Strelley Pool Formation, Pilbara Craton, Western Australia. Geological Survey of Western Australia.
Hickman, A.H., 2012. Review of the Pilbara Craton and Fortescue Basin, Western Australia: Crustal evolution providing environments for early life. Island Arc 21, 1-31.
Hickman, A.H., 2016. Northwest Pilbara Craton: a record of 450 million years in the growth of Archean continental crust, Report. Geological Survey of Western Australia, p. 104.
Hickman, A.H., Van Kranendonk, M.J., 2004. Diapiric processes in the formation of Archaean continental crust, East Pilbara Granite-Greenstone Terrane, Australia, in: Eriksson, P.G., Altermann, W., Nelson, D.R., Mueller, W.U., Catuneanu, O. (Eds.), The Precambrian Earth: Tempos and Events. Elsevier, Amsterdam, pp. 54-75.
Hickman, A.H., Van Kranendonk, M.J., 2012. Early Earth evolution: evidence from the 3.5–1.8 Ga geological history of the Pilbara region of Western Australia. Episodes 35, 283-297.
Jahn, B.-m., Glikson, A.Y., Peucat, J.J., Hickman, A.H., 1981. REE geochemistry and isotopic data of Archean silicic volcanics and granitoids from the Pilbara Block, Western Australia: implications for the early crustal evolution. Geochimica et Cosmochimica Acta 45, 1633-1652.
Johnson, T.E., Brown, M., Gardiner, N.J., Kirkland, C.L., Smithies, R.H., 2017. Earth's first stable continents did not form by subduction. Nature.
Johnson, T.E., Brown, M., Goodenough, K.M., Clark, C., Kinny, P.D., White, R.W., 2016. Subduction or sagduction? Ambiguity in constraining the origin of ultramafic–mafic bodies in the Archean crust of NW Scotland. Precambrian Research 283, 89-105.
Johnson, T.E., Brown, M., Kaus, B.J.P., VanTongeren, J.A., 2014. Delamination and recycling of Archaean crust caused by gravitational instabilities. Nature Geoscience 7, 47-52.
Kamber, B.S., 2015. The evolving nature of terrestrial crust from the Hadean, through the Archaean, into the Proterozoic. Precambrian Research 258, 48-82.
Kemp, A.I., Vervoort, J.D., Smithies, R.H., Hickman, A.H., Van Kranendonk, M.J., 2011. Recoupling the Nd-Hf isotope record of the early Earth? Evidence from the Pilbara craton, Western Australia, American Geophysical Union Fall Meeting 2011.
Kemp, A.I.S., Hickman, A.H., Kirkland, C.L., Vervoort, J.D., 2015. Hf isotopes in detrital and inherited zircons of the Pilbara Craton provide no evidence for Hadean continents. Precambrian Research 261, 112-126.
Kinny, P.D., 2000. U-Pb dating of rare-metal (Sn-Ta-Li) mineralized pegmatites in Western Australia by SIMS analysis of tin and tantalum-bearing ore minerals, Beyond 2000, New Frontiers in Isotope Geoscience, pp. 113-116.
Kirkland, C.L., Johnson, S.P., Smithies, R.H., Hollis, J.A., Wingate, M.T.D., Tyler, I.M., Hickman, A.H., Cliff, J.B., Tessalina, S., Belousova, E.A., Murphy,

R.C., 2013. Not-so-suspect terrane: Constraints on the crustal evolution of the Rudall Province. Precambrian Research 235, 131-149.
Kirkland, C.L., Smithies, R.H., Spaggiari, C.V., 2015. Foreign contemporaries – Unravelling disparate isotopic signatures from Mesoproterozoic Central and Western Australia. Precambrian Research 265, 218-231.
Kloppenburg, A., 2003. Structural evolution of the Marble Bar Domain, Pilbara granite-greenstone terrain, Australia: The role of Archaean mid- crustal detachments. Utrecht University, Utrecht.
Krapez, B., 1993. Sequence stratigraphy of the Archaean supracrustal belts of the Pilbara Block, Western Australia. Precambrian Research 60, 1-45.
Krapez, B., Eisenlohr, B., 1998. Tectonic Settings of Archaean (3325-2775 Ma) crustal-supracrustal belts in the West Pilbara Block. Precambrian Research 88, 173-205.
Kröner, A., Alexeiev, D.V., Hegner, E., Rojas-Agramonte, Y., Corsini, M., Chao, Y., Wong, J., Windley, B.F., Liu, D., Tretyakov, A.A., 2012. Zircon and muscovite ages, geochemistry, and Nd–Hf isotopes for the Aktyuz metamorphic terrane: Evidence for an Early Ordovician collisional belt in the northern Tianshan of Kyrgyzstan. Gondwana Research 21, 901-927.
McNaughton, N.J., Green, M.D., Compston, W., Williams, I.S., 1988. Are anorthositic rocks basement to the Pilbara Craton?, Geological Society of Australia, pp. 272-273.
Mole, D.R., Fiorentini, M.L., Thebaud, N., Cassidy, K.F., McCuaig, T.C., Kirkland, C.L., Romano, S.S., Doublier, M.P., Belousova, E.A., Barnes, S.J., Miller, J., 2014. Archean komatiite volcanism controlled by the evolution of early continents. Proc Natl Acad Sci U S A 111, 10083-10088.
Moyen, J.-F., 2011. The composite Archaean grey gneisses: Petrological significance, and evidence for a non-unique tectonic setting for Archaean crustal growth. Lithos 123, 21-36.
Moyen, J.-F., Martin, H., 2012. Forty years of TTG research. Lithos 148, 312-336.
Moyen, J.-F., Stevens, G., Kisters, A.F.M., Belcher, R.W., 2007. TTG Plutons of the Barberton Granitoid-Greenstone Terrain, South Africa, in: Van Kranendonk, M.J., Smithies, R.H., Bennett, V.C. (Eds.), Earth's Oldest Rocks. Developments in Precambrian Geology. Elsevier, pp. 607-667.
Naeraa, T., Schersten, A., Rosing, M.T., Kemp, A.I., Hoffmann, J.E., Kokfelt, T.F., Whitehouse, M.J., 2012. Hafnium isotope evidence for a transition in the dynamics of continental growth 3.2 Gyr ago. Nature 485, 627-630.
Nebel, O., Campbell, I.H., Sossi, P.A., Van Kranendonk, M.J., 2014. Hafnium and iron isotopes in early Archean komatiites record a plume-driven convection cycle in the Hadean Earth. Earth and Planetary Science Letters 397, 111-120.
Nelson, D.R., 1999a. Banded biotite tonalite gneiss, 6 Mile Well (No. 345), Geochronology Record. Geological Survey of Western Australia.
Nelson, D.R., 1999b. Compilation of Geochronology Data, 1988. Geological Survey of Western Australia.
Pawley, M.J., Van Kranendonk, M.J., Collins, W.J., 2004. Interplay between deformation and magmatism during doming of the Archaean Shaw Granitoid Complex, Pilbara Craton, Western Australia. Precambrian Research 131, 213-230.

Payne, J.L., McInerney, D.J., Barovich, K.M., Kirkland, C.L., Pearson, N.J., Hand, M., 2016. Strengths and limitations of zircon Lu-Hf and O isotopes in modelling crustal growth. Lithos 248-251, 175-192.
Roberts, N.M.W., 2012. Increased loss of continental crust during supercontinent amalgamation. Gondwana Research 21, 994-1000.
Scherer, E.E., Munker, C., Mezger, K., 2001. Calibration of the Lutetium-Hafnium Clock. Science 293, 683-686.
Scherer, E.E., Whitehouse, M., Munker, C., 2007. Zircon as a Monitor of Crustal Growth. Elements 3, 19-24.
Smith, J.B., Barley, M.E., Groves, D.I., Krapez, B., McNaughton, N.J., Bickle, M.J., Chapman, H.J., 1998. The Sholl Shear Zone, West Pilbara: evidence for a domain boundary structure from integrated tectonic analyses, SHRIMP U–Pb dating and isotopic and geochemical data of granitoids. Precambrian Research 88, 143-171.
Smithies, R.H., 2000. The Archaean tonalite-trondhjemite-granodiorite (TTG) series is not an analogue of Cenozoic adakite. Earth and Planetary Science Letters 182, 115-125.
Smithies, R.H., Champion, D.C., Cassidy, K.F., 2003. Formation of Earth's early Archaean continental crust. Precambrian Research 127, 89-101.
Smithies, R.H., Champion, D.C., Sun, S.s., 2004. Evidence for Early LREE-enriched Mantle Source Regions: Diverse Magmas from the
c. 3.0 Ga Mallina Basin, Pilbara Craton, NW Australia. Journal of Petrology 45, 1515-1537.
Smithies, R.H., Champion, D.C., Van Kranendonk, M.J., 2009. Formation of Paleoarchean continental crust through infracrustal melting of enriched basalt. Earth and Planetary Science Letters 281, 298-306.
Smithies, R.H., Champion, D.C., Van Kranendonk, M.J., Hickman, A.H., 2007a. Geochemistry of Volcanic Rocks of the Northern Pilbara Craton Western Australia. Geological Survey of Western Australia, Perth.
Smithies, R.H., Van Kranendonk, M.J., Champion, D.C., 2005. It started with a plume – early Archaean basaltic proto-continental crust. Earth and Planetary Science Letters 238, 284-297.
Smithies, R.H., Van Kranendonk, M.J., Champion, D.C., 2007b. The Mesoarchean emergence of modern-style subduction. Gondwana Research 11, 50-68.
Tessalina, S.G., Bourdon, B., Van Kranendonk, M., Birck, J.-L., Philippot, P., 2010. Influence of Hadean crust evident in basalts and cherts from the Pilbara Craton. Nature Geoscience 3, 214-217.
Thébaud, N., Rey, P.F., 2013. Archean gravity-driven tectonics on hot and flooded continents: Controls on long-lived mineralised hydrothermal systems away from continental margins. Precambrian Research 229, 93-104.
Thorpe, R.I., Hickman, A.H., Davis, D.W., Mortensen, J.K., Trendall, A.F., 1992a. Constraints to models for Archaean lead evolution from precise zircon U-Pb geochronology for the Marble Bar region, Pilbara Craton, Western Australia. Geology Department, University of Western Australia, pp. 395-407.
Thorpe, R.I., Hickman, A.H., Davis, D.W., Mortensen, J.K., Trendall, A.F., 1992b. U-Pb zircon geochronology of Archaean felsic units in the Marble Bar region, Pilbara Craton, Western Australia. Precambrian Research 56, 169-189.

Tomlinson, K.Y., Stott, G.M., Percival, J.A., Stone, D., 2004. Basement terrane correlations and crustal recycling in the western Superior Province: Nd isotopic character of granitoid and felsic volcanic rocks in the Wabigoon subprovince, N. Ontario, Canada. Precambrian Research 132, 245-274.

Van Kranendonk, M.J., 1998. Litho-tectonic and structural map components of the North Shaw 1:100 000 sheet, Archaean Pilbara Craton, Annual Review, Geological Survey of Western Australia, pp. 63-70.

Van Kranendonk, M.J., 2010. Two types of Archean continental crust: Plume and plate tectonics on early Earth. American Journal of Science 310, 1187-1209.

Van Kranendonk, M.J., Collins, W.J., Hickman, A., Pawley, M.J., 2004. Critical tests of vertical vs. horizontal tectonic models for the Archaean East Pilbara Granite–Greenstone Terrane, Pilbara Craton, Western Australia. Precambrian Research 131, 173-211.

Van Kranendonk, M.J., Hickman, A.H., Smithies, R.H., Nelson, D.R., Pike, G., 2002. Geology and Tectonic Evolution of the Archean North Pilbara Terrain, Pilbara Craton, Western Australia. Economic Geology 97, 695-732.

Van Kranendonk, M.J., Hickman, A.H., Smithies, R.H., Williams, I.R., Bagas, L., Farrell, T.R., 2006. Revised lithostratigraphy of Archean supracrustal and intrusive rocks in the northern Pilbara Craton, Western Australia.

Van Kranendonk, M.J., Hugh Smithies, R., Hickman, A.H., Champion, D.C., 2007a. Review: secular tectonic evolution of Archean continental crust: interplay between horizontal and vertical processes in the formation of the Pilbara Craton, Australia. Terra Nova 19, 1-38.

Van Kranendonk, M.J., Hugh Smithies, R., Hickman, A.H., Wingate, M.T.D., Bodorkos, S., 2010. Evidence for Mesoarchean (~3.2Ga) rifting of the Pilbara Craton: The missing link in an early Precambrian Wilson cycle. Precambrian Research 177, 145-161.

Van Kranendonk, M.J., Kirkland, C.L., Cliff, J., 2015. Oxygen isotopes in Pilbara Craton zircons support a global increase in crustal recycling at 3.2Ga. Lithos 228-229, 90-98.

Van Kranendonk, M.J., Smithies, R.H., Griffin, W.L., Huston, D.L., Hickman, A.H., Champion, D.C., Anhaeusser, C.R., Pirajno, F., 2014. Making it thick: a volcanic plateau origin of Palaeoarchean continental lithosphere of the Pilbara and Kaapvaal cratons. Geological Society, London, Special Publications 389, 83-111.

Van Kranendonk, M.J., Smithies, R.H., Hickman, A.H., Champion, D.C., 2007b. Paleoarchean Development of a Continental Nucleus: The East Pilbara Terrane of the Pilbara Craton, Western Australia, in: Van Kranendonk, M.J., Smithies, R.H., Bennett, V.C. (Eds.), Earth's Oldest Rocks, pp. 307-337.

Wei, X., Feng, Y.G., ZHao, J.X., 2014. Plume-Lithosphere Interaction in the Generation of the Tarim Large Igneous Province, NW China: Geochronological and Geochemical Constraints. American Journal of Science 314, 314-356.

Williams, I.R., 2000. Geology of the Warrawagine 1:100 000 sheet. Geological Survey of Western Australia.

Williams, I.S., Collins, W.J., 1990. Granite-greenstone terranes in the Pilbara Block, Australia, as coeval volcano-plutonic complexes; evidence from U-Pb zircon dating of the Mount Edgar Batholith. Earth and Planetary Science Letters 97, 41-53.

Woodhead, J., Hergt, J., Shelley, M., Eggins, S., Kemp, R., 2004. Zircon Hf-isotope analysis with an excimer laser, depth profiling, ablation of complex geometries, and concomitant age estimation. Chemical Geology 209, 121-135.

Figure and Table Captions

Figure 1: Terrane map of the northern part of the Pilbara Craton in Western Australia, showing the East Pilbara Terrane, the West Pilbara Superterrane, the Kurrana Terrane, and the De Grey Supergroup (MB = Mallina Basin; MCB = Mosquito Creek basin cover. Shear zones: MLSZ = Maitland Shear Zone; TTSZ = Tabba Tabba Shear Zone. After Hickman (2016).

Figure 2: Generalized regional lithostratigraphy of the Pilbara Supergroup, East Pilbara Craton, showing unconformities and volcanic cycles, and interpreting episodic consequences of diapiric doming. After Hickman (2012).

Figure 3: Schematic map of large-scale structures of the East Pilbara Terrane. All domes are separated by minor faults. LR-WS = the sinistral transpressional Lalla Rookh–Western Shaw structural corridor.

Figure 4: Geological map of the Mount Edgar Dome showing the major supersuites and their subdivisions. Contacts between the Marble Bar greenstone belt and the greenstone belts of the Muccan and Corunna Downs are major faults. Note the concentration of oldest granitic units along the southwest and southeast margins of the granitic complex.

Figure 5: Sample locality map for the Mount Edgar Dome for this study.

Figure 6: εHf evolution diagrams for the Mount Edgar Dome samples. A: Focus on >3.2 Ga Mount Edgar magmatism; B: All Edgar data. Blue shading shows Hf evolution line defined by a $^{176}Lu/^{177}Hf$ ratio of 0.010. Uncertainties are shown at 1σ. A blanket error of 7 Ma is derived from the mean value of all U-Pb age errors.

Figure 7: Isotope evolution plots showing (a) Nd T_{DM}^2 ages and (b) εNd(t) versus magmatic ages for the Pilbara Craton. The East Pilbara Terrane shows approximately constant T_{DM}^2 and largely decreasing εNd with decreasing magmatic age, consistent with reworking of existing crust with time. The exception to this is the late-stage 2.9–2.8 Ga magmatism in the western part of the East Pilbara Terrane, which shows the influence of a more juvenile component, interpreted as resulting from the growth of the West Pilbara Terrane.

Figure 8: εHf isotopic map for the Mount Edgar Dome, delineated by geological boundaries, and coloured by median εHf per supersuite. A general rim-core trend from juvenile to more evolved Hf signal is observed, consistent with an increasing dominance of reworking of existing crustal material with time, reflected in the younger supersuites, which core the dome.

Figure 9: Plot of whole-rock K2O (wt%) versus the median εHf value for that sample, for Palaeoarchaean supersuites. No discernable trend on a per-supersuite basis is observed, although overall the more isotopically evolved supersuite (Cleland, negative εHf) is more K_2O-rich, as would be expected with reworking driving chemical differentiation. Whole-rock data extracted from the Geological Survey of Western Australia's (GSWA) geochronology and geochemistry online databases (http://www.dmp.wa.gov.au/geochron and http://www.dmp.wa.gov.au/geochem).

Figure 10: Modelling the Hf isotope evolution of the > 3.2 Ga Mount Edgar Dome samples. The medians of initial $^{176}Hf/^{177}Hf$ and magmatic age for the three supersuites are shown: Tambina (M1: 3442 Ma, $^{176}Hf/^{177}Hf$ = 0.280596); Emu Pool (M2: 3308 Ma, $^{176}Hf/^{177}Hf$ = 0. 280661); and Cleland (M3: 3235 Ma, $^{176}Hf/^{177}Hf$ = 0.280646). Evolution lines from M1, defined by a source $^{176}Lu/^{177}Hf$ value of 0.010 (green) and 0.015 (grey) are plotted. The values E2 and E3 represent the "evolved" end-member composition lying on the 0.010 evolution array, i.e. that with the evolving M2 composition. J2 and J3 are the juvenile, i.e. Depleted Mantle, end-member compositions for the M2 and M3 respectively. This modelling suggests the Hf isotope composition of M2 cannot be attained solely through reworking of M1 crust, and requires an input of material with a more juvenile signature. Mass balance calculation between E2, M2 and J2 implies a juvenile input of some 22% by mass is required. Similarly, M3 requires minimal (5%) input of a J3 DM source.

Figure 11: Plotting whole-rock K_2O and K_2O/Na_2O against $^{207}Pb/^{206}Pb$

magmatic age for East Pilbara TTGs and granites. This shows a general trend towards more K_2O-rich magmatism, consistent with differentiation processes. Points in grey are individual whole-rock analysis of East Pilbara granitoids, extracted from the same GSWA databases as per Fig. 9. The orange line is a curve fitted to the East Pilbara data. The average sodic TTG line uses data collated from Moyen (2011).

Figure 12: Sm-Nd isotopic maps for the Pilbara Terrane. Thick black lines are faults and thin black lines are tectonic unit boundaries. Abbreviations for tectonic units: FB = Fortescue Basin; HB = Hamersley Basin; YU = Yule dome; CA = Carlindi dome; MU = Muccan dome; ME = Mount Edgar dome; CO = Corunna Downs dome; SH = Shaw dome; TA = Tambourah dome; WA = Warrawagine dome. Data source is the tabulated Sm-Nd isotopic data provided in Supplementary Table S1, which is a compilation of both unpublished GSWA data plus additional data from Arndt et al. (2001), Champion (2013), Gruau et al. (1987) and Hamilton et al. (1981).

Table 1: Summary of Mount Edgar samples analyzed for Hf and Nd isotopes, including locations and simple descriptions. Quoted U-Pb magmatic ages are from the appropriate GSWA reports (Geochronological references are given in Supplementary Table 1). εHf and T_{DM}^2 are medians of the individual analyses, excluding those interpreted as inherited. A $^{176}Lu/^{177}Hf$ ratio of 0.010 was used for the calculation of Hf model ages (T_{DM}^2). See Appendix A for information on calculation of εHf and εNd.

Table 2: Compilation of Zircon Lu-Hf isotope data from the Mount Edgar Dome samples.

Table 3: Summary of whole-rock Sm-Nd data for samples from the Pilbara Craton. Age uncertainties are 1σ.

Supplementary Data:

Two additional data tables are provided in Excel format:

Table S1: Full Sm-Nd data from across the East Pilbara Terrane, including the new data presented here, and used to make the Nd isotope maps.

Table S2: U-Pb geochronology references for the Mount Edgar age data.

Appendix A: Analytical Methodologies

Lu-Hf Geochronology Methodology

Hafnium isotope analyses were conducted on previously dated zircons using a New Wave/Merchantek LUV213 laser-ablation microprobe, attached to a Nu Plasma multi-collector inductively coupled plasma mass spectrometer (LA-MC-ICPMS) at Macquarie University. The method has been discussed in detailed elsewhere (Griffin et al., 2000). Analyses involved a laser beam diameter of ca. 40 µm with ablation pits 40–60 µm deep. The ablated sample material was transported from the laser cell to the ICP–MS torch in a helium gas flow. Interference of ^{176}Lu on ^{176}Hf was corrected by measurement of the interference-free ^{175}Lu and using an invariant $^{176}Lu/^{175}Lu$ correction factor. Isobaric interference of ^{176}Yb on ^{176}Hf was corrected by measurement of the interference-free ^{172}Yb isotope and using the $^{176}Yb/^{172}Yb$

ratio to calculate the intensity of interference free ^{176}Yb. The appropriate value of $^{176}Yb/^{172}Yb$ was determined by successive doping of the JMC475 Hf standard with various amounts of Yb.

Analysis of samples in the Pilbara dataset were conducted over five sessions. Zircons from the Mud Tank carbonatite locality were analyzed, together with the samples, as a measure of the accuracy of the results. Most of the data and the mean $^{176}Hf/^{177}Hf$ value of Mudtank zircon in each session (session 1: 0.282525 ± 18, n = 50; session 2: 0.282542 ± 28, n = 19; session 3; 0.282523 ± 15, n = 17; session 4; 0.282522 ± 31, n= 39; session 5; 0.282539 ± 52, n= 76) are within 2 standard deviations (2σ) of the recommended value (0.282522 ± 42 (2σ) (Griffin et al., 2007). Temora-2 zircon was run as an independent check on the accuracy of the Yb correction. Temora zircon has an average $^{176}Yb/^{177}Hf$ ratio of 0.04, which is similar to the mean $^{176}Yb/^{177}Hf$ ratio of zircon in this study (0.03). The average $^{176}Hf/^{177}Hf$ ratio for Temora-2 in each session (session 1: 0.282681 ± 20, n= 6; session 2: 0.282695 ± 28, n = 4; session 3: 0.282683 ± 26, n = 11; session 4: 0.282696 ± 27, n = 14; session 5: 0.282703 ± 31 n = 33) was consistent with the published value for the Temora-2 standard (0.282687 ± 24; LA-ICPMS; Hawkesworth and Kemp (2006)). Calculation of εHf values employs the decay constant of Scherer et al. (2001) and the CHUR values of Blichert-Toft and Albarède (1997). Full Hf analytical data is presented in Table 2.

Sm-Nd Geochronology Methodology

Neodymium isotopes are compiled from published sources and new analyses (Table S1). New neodymium isotope analyses were performed

on whole rock samples from the Pilbara using a Nu Plasma multi-collector ICPMS at the University of Queensland following procedures documented in Wei et al. (2014), except that the samples in this study were digested in high-pressure Teflon bombs at 180°C to ensure complete digestion of zircons. The measured $^{143}Nd/^{144}Nd$ ratios were corrected for mass fractionation to $^{146}Nd/^{144}Nd = 0.7219$. The AMES Nd metal standard (Wei et al., 2014) run throughout the course of these analyses returned a $^{143}Nd/^{144}Nd = 0.511966 \pm 7$ (n = 12, 2σ) identical to the accepted value. International rock standards BCR-2 and JG-3 processed together with our samples gave $^{143}Nd/^{144}Nd$ ratios of 0.512635 ± 6 (2σ) and 0.512625 ± 7 (2σ), respectively. Total Nd procedural blanks run in the lab typically range from 20–100 pg, which is considered negligible compared to the total quantity of Nd in the samples. A table of the new Nd isotopic values reported here is provided in Table 2.

Appendix B: Discussion of Isotope Results

Tambina Supersuite

Fifty-six Tambina Supersuite (3451–3416 Ma) analyses with magmatic $^{207}Pb/^{206}Pb$ crystallization ages ranging from 3481 to 3406 Ma, have minimum and maximum εHf of -1.8 and +3.9, respectively, and a median εHf of +1.0. Four samples from the Tambina Supersuite have older ages, interpreted as representing inheritance; a biotite microtonalite (178036; 3468 and 3481 Ma), a biotite granodiorite (169041; 3461-3468 Ma), a metamonzonite (178079; 3466 and 3467 Ma), and a biotite granodiorite (178100; 3469 Ma), These four samples have εHf ranging from +0.4 to +2.3, the most juvenile Hf isotope signature of the Mt Edgar samples.

Two samples of the Tambina Supersuite (169041 and 178036) were analysed for whole-rock Sm–Nd isotopes. and gave calculated εd values of -0.03 and +0.40, respectively.

Emu Pool Supersuite

159 Emu Pool Supersuite (3324–3277 Ma) analyses lie within this age range, with a max of 3340 Ma and min of 3271 Ma. εHf range from +3.9 to -5.0, with a median of 0.0. Two samples from the Emu Pool Supersuite have older ages, interpreted as representing inheritance; a biotite granodiorite (169042; 3451-3476 Ma), and a biotite monzogranite (178095; 3346 Ma), which yield εHf of -0.4 and +0.9 respectively.

One sample of the Emu Pool Supersuite (169042) was analysed for whole-rock Sm–Nd isotopes. giving a calculated εNd value of -1.44.

Cleland Supersuite

Sixty-one Cleland Supersuite (3260–3200 Ma) analyses have magmatic ages ranging from 3256 to 3208 Ma. These samples have a range of εHf of between +1.0 to -5.6, and a non-normal distribution with a mean of -2.2. Five samples from the Cleland Supersuite also have older zircon ages, interpreted as inheritance. These ages range from 3334 to 3265 Ma, and have εHf ranging from -2.5 to +0.6, with a mean of -1.6.

Split Rock Supersuite

One sample (169044), a muscovite-biotite monzogranite from the Split Rock Supersuite (2900–2800 Ma), defines a much younger grouping, with an age range of 2887-2819 Ma. Six analysis yield a range of εHf from -

1.0 to -6.7, and a median of -4.0. This late stage set of analyses represents the most evolved Hf signature analyzed in the Mount Edgar samples.

The sample from the Split Rock Supersuite was also analysed for whole-rock Sm-Nd isotopes, giving a calculated εNd value of -7.08.

ample ID	at	ong	ge Ma (2σ)	Hf (1σ)	$_{DM}^{2}$ Ga	Nd	upersuite	Lithology
42977.1	21.14646	19.9039	313 ± 3	0.3 ± 1.3	.60		plit Rock	monzogranite magnetite
42980.1	21.20119	20.15471	243 ± 4	1.3 ± 1.6	.59		leland monzogranite	
42983.1	21.19507	20.08443	241 ± 3	2.9 ± 1.7	.68		leland	biotite monzogranite
69034.1	21.21136	20.26109	246 ± 3	2.1 ± 1.4	.63		leland	biotite monzogranite
78076.1	21.03321	19.99048	223 ± 3	3.1 ± 1.1	.66		leland	biotite monzogranite
78078.1	21.06877	19.97465	234 ± 2	0.5 ± 1.5	.55		leland	biotite monzogranite
78094.1	21.13259	20.11905	243 ± 5	0.9 ± 2.1	.61		leland	biotite monzogranite

42984.1	21.18508	20.03054	312 ± 4	.5 ± 0.9	.57		mu Pool	pegmatite-banded orthogneiss
42985.1	21.18813	19.96307	315 ± 5	.6 ± 0.9	.60		mu Pool	biotite tonalite
69038.1	21.26757	20.22047	315 ± 2	1.0 ± 0.7	.63		mu Pool	biotite-hornblende granodiorite
69040.1	21.30784	20.25959	314 ± 6	0.1 ± 1.4	.63		mu Pool	biotite metagranodiorite gneiss
69042.1	21.39186	20.21416	323 ± 9	0.3 ± 1.7	.61	1.4	mu Pool	biotite granodiorite
69045.1	21.24514	19.84681	307 ± 3	.7 ± 0.8	.54		mu Pool	biotite tonalite
69046.1	21.25022	19.84537	310 ± 4	0.5 ± 1.2	.60		mu Pool	biotite metadiorite gneiss
78037.1	21.23006	19.88464	313 ± 2	1.3 ± 1.5	.65		mu Pool	biotite granodiorite
78075.1	21.11103	19.90478	303 ± 2	0.4 ± 1.3	.58		mu Pool	biotite granodiorite

78077.1	21.06919	19.97391	315 ± 3	.1 ± 0.9	.53		mu Pool	biotite tonalite
78095.1	21.02659	20.061	310 ± 5	.3 ± 2.2	.60		mu Pool	biotite monzogranite
78096.1	21.0584	20.24505	297 ± 4	0.2 ± 1.0	.57		mu Pool	biotite monzogranite
78098.1	21.0552	20.27908	302 ± 8	.2 ± 1.4	.56		mu Pool	biotite monzogranite
78099.1	21.00534	20.19847	308 ± 4	.3 ± 1.1	.51		mu Pool	biotite granodiorite
69031.1	21.21482	20.01294	430 ± 4	1.1 ± 1.8	.62		ambina	biotite metatonalite gneiss
69041.1	21.38994	20.19107	466 ± 4	1.2 ± 1.8	.74	.4	ambina	biotite granodiorite
78036.1	21.3017	19.89693	435 ± 4	.8 ± 1.8	.64	0.0	ambina	biotite microtonalite
78079.1	21.01655	19.8813	416 ± 8	.8 ± 1.1	.64		ambina	leucocratic metamonzogranite gneiss

78100.1	21.36039	20.05042	435 ± 3	.1 ± 1.0	.62		ambina		leucotonalite muscovite-biotite
69044.1	21.17173	20.01082	831 ± 12	2.7 ± 2.5	.46	7.1	plit Rock	monzogranite	

ample ID	ample no	ge (Ma)	σ	$^{76}Hf/^{177}Hf$ (meas)	σ	$^{76}Lu/^{177}Hf$ meas)	$^{76}Hf/^{177}Hf$ nitial	Hf	σ	$_{DM}^{2}$	nherited
	Cleland										
Supersuite											
42977.1	42977-10.1	325		.280714	.000011	.000756	.280666	.6	.39	.56	
42977.1	42977-13.1	265		.280692	.000011	.000831	.280640	1.7	.39	.63	

42977.1	42977-16.1	266		.280718	.000025	.000495	.280687	.0	.88	.54
42977.1	42977-22.1	236		.280700	.000010	.000601	.280663	1.6	.33	.60
42977.1	42977-27.1	243		.280651	.000018	.000451	.280623	2.8	.63	.67
42977.1	42977-02.1	314		.280696	.000007	.000473	.280666	.4	.26	.56
42977.1	42977-04.1	319		.280666	.000010	.000738	.280619	1.2	.35	.65
42977.1	42977-19.1	292		.280712	.000013	.000502	.280680	.4	.46	.55
42977.1	42977-24.1	303	3	.280712	.000019	.000886	.280656	0.2	.67	.59
42977.1	42977-26.1	311		.280741	.000014	.000694	.280697	.4	.49	.51
42977.1	42977-28.1	319		.280692	.000013	.000756	.280644	0.3	.46	.60

42980.1	42980-06.1	244	.280755	.000021	.001455	.280664	1.3	.74	.59
42980.1	42980-09.1	239	.280704	.000021	.000930	.280646	2.1	.74	.63
42980.1	42980-12.1	245	.280691	.000017	.001507	.280597	3.7	.60	.71
42980.1	42980-16.1	254	.280763	.000020	.001110	.280694	.0	.70	.54
42980.1	42980-18.1	251	.280703	.000018	.000814	.280652	1.6	.63	.61
42980.1	42980-23.1	236	.280765	.000013	.001436	.280676	1.1	.46	.58
42980.1	42980-25.1	246	.280694	.000013	.000428	.280667	1.2	.46	.59
42980.1	42980-03.1	296	.280655	.000011	.000475	.280625	1.5	.39	.64
42980.1	42980-15.1	306	.280694	.000012	.000512	.280661	.0	.42	.57

42980.1	42980-21.1	307	.280780	.000012	.000719	.280734	.7	.42	.44
42983.1	42983-02.1	235	.280720	.000054	.001337	.280637	2.5	.89	.65
42983.1	42983-03.1	236	.280637	.000026	.001132	.280567	5.0	.91	.77
42983.1	42983-04.1	247	.280658	.000034	.000987	.280596	3.7	.19	.71
42983.1	42983-06.1	221	.280702	.000020	.000986	.280641	2.7	.70	.64
42983.1	42983-08.1	234	.280756	.000023	.001178	.280683	0.9	.81	.56
42983.1	42983-10.1	245	.280623	.000044	.001250	.280545	5.5	.54	.81
42983.1	42983-11.1	246	.280721	.000037	.001302	.280640	2.1	.30	.64
42983.1	42983-14.1	243	.280753	.000036	.001274	.280674	1.0	.26	.58

42983.1	42983-16.1	232		.280698	.000033	.001243	.280621	3.2	.16	.68
42983.1	42983-17.1	256	2	.280652	.000036	.000630	.280613	2.9	.26	.68
42983.1	42983-18.1	242		.280623	.000031	.000474	.280593	3.9	.09	.72
42983.1	42983-20.1	239		.280640	.000023	.000776	.280592	4.0	.81	.73
42983.1	42983-21.1	247	1	.280757	.000017	.000794	.280707	.3	.60	.51
69034.1	69034-02.1	236	1	.280710	.000017	.000912	.280653	1.9	.60	.62
69034.1	69034-04.1	237		.280761	.000018	.001485	.280669	1.3	.63	.59
69034.1	69034-05.1	250		.280713	.000019	.000793	.280663	1.2	.67	.59
69034.1	69034-06.1	238		.280758	.000028	.001680	.280653	1.8	.98	.61

69034.1	69034-09.1	240		.280701	.000019	.000889	.280646	2.1	.67	.63
69034.1	69034-10.1	251		.280659	.000028	.001405	.280571	4.5	.98	.76
69034.1	69034-11.1	248		.280659	.000009	.001883	.280541	5.6	.33	.81
69034.1	69034-16.1	246		.280686	.000023	.001627	.280584	4.1	.81	.74
69034.1	69034-17.1	236	8	.280682	.000009	.000578	.280646	2.2	.32	.63
69034.1	69034-22.1	256		.280691	.000016	.001323	.280608	3.0	.56	.69
69034.1	69034-25.1	251		.280652	.000013	.000959	.280592	3.7	.46	.72
69034.1	69034-08.1	303		.280741	.000014	.001011	.280677	.5	.49	.55
78076.1	78076-01.1	222		.280730	.000013	.001595	.280631	3.0	.46	.66

78076.1	78076-03.1	227		.280709	.000013	.001712	.280603	3.9	.46	.71
78076.1	78076-06.1	214	2	.280774	.000029	.002060	.280647	2.6	.02	.64
78076.1	78076-08.1	223		.280733	.000011	.001889	.280616	3.5	.39	.69
78076.1	78076-10.1	208		.280766	.000011	.002140	.280634	3.2	.39	.66
78076.1	78076-13.1	222		.280770	.000009	.001616	.280670	1.6	.32	.59
78076.1	78076-16.1	218		.280695	.000011	.001024	.280632	3.1	.39	.66
78076.1	78076-17.1	229		.280733	.000012	.000968	.280673	1.4	.42	.58
78076.1	78076-19.1	223		.280689	.000010	.000868	.280635	2.8	.34	.65
78076.1	78076-21.1	220		.280778	.000011	.000952	.280719	.1	.39	.50

78076.1	78076-23.1	226	.280677	.000011	.001015	.280614	3.5	.39	.69
78076.1	78076-25.1	228	.280679	.000010	.000972	.280619	3.3	.35	.68
78076.1	78076-05.1	307	.280711	.000020	.002194	.280571	3.2	.70	.74
78078.1	78078-03.1	241	.280694	.000010	.000561	.280659	1.6	.35	.60
78078.1	78078-09.1	238	.280729	.000008	.000467	.280700	0.2	.28	.53
78078.1	78078-12.1	237	.280732	.000009	.000590	.280695	0.4	.32	.54
78078.1	78078-14.1	230	.280737	.000010	.000713	.280693	0.6	.35	.55
78078.1	78078-16.1	231	.280760	.000030	.001011	.280697	0.5	.05	.54
78078.1	78078-21.1	233	.280702	.000030	.000642	.280662	1.7	.05	.60

78078.1	78078-05.1	307	.280663	.000024	.000579	.280626	1.2	.84	.64
78078.1	78078-07.1	286	.280716	.000006	.000545	.280682	.3	.22	.55
78078.1	78078-10.1	303	.280672	.000009	.000645	.280631	1.1	.30	.63
78078.1	78078-13.1	297	.280790	.000010	.000875	.280735	.4	.35	.44
78078.1	78078-19.1	294	.280780	.000018	.000626	.280740	.6	.63	.44
78094.1	78094-01.1	247	.280774	.000018	.001620	.280673	0.9	.63	.58
78094.1	78094-02.1	243	.280660	.000019	.000294	.280642	2.2	.67	.63
78094.1	78094-03.1	229	.280669	.000014	.000932	.280611	3.6	.49	.69
78094.1	78094-04.1	235	.280763	.000017	.001265	.280684	0.8	.60	.56

78094.1	78094-08.1	239		.280780	.000150	.000386	.280756	.8	.25	.43
78094.1	78094-12.1	238		.280670	.000010	.000460	.280641	2.3	.35	.64
78094.1	78094-15.2	231		.280683	.000012	.000507	.280652	2.1	.42	.62
78094.1	78094-17.1	265		.280720	.000011	.001242	.280642	1.6	.39	.63
78094.1	78094-18.1	223	1	.280694	.000040	.000971	.280634	2.9	.40	.66
78094.1	78094-20.1	243	6	.280839	.000046	.001338	.280756	.9	.61	.43
78094.1	78094-23.1	213		.280610	.000023	.000483	.280580	5.0	.81	.76
78094.1	78094-25.1	334		.280623	.000012	.000802	.280572	2.5	.42	.73
78094.1	78094-09.1	302		.280771	.000015	.001131	.280699	.3	.53	.51

78094.1	78094-14.1	311	.280667	.000011	.000292	.280648	0.3	.39	.60
78094.1	78094-16.2	308	.280730	.000017	.001024	.280665	.2	.60	.57
78094.1	78094-10.1	450	.280679	.000015	.001543	.280576	.4	.53	.67
	Emu Pool								
Supersuite									
42984.1	42984-01.1	302	.280732	.000026	.000763	.280684	.7	.91	.54
42984.1	42984-02.1	302	.280646	.000013	.000568	.280610	1.9	.46	.67
42984.1	42984-03.1	319	.280718	.000014	.000680	.280675	.8	.49	.55
42984.1	42984-05.1	271	.280720	.000018	.000742	.280673	0.4	.63	.57
42984.1	42984-08.1	315	.280678	.000010	.000544	.280643	0.4	.35	.60

42984.1	42984-09.1	290	.280728	.000015	.000674	.280685	.5	.53	.54
42984.1	42984-11.1	294	.280689	.000010	.000689	.280645	0.8	.35	.61
42984.1	42984-13.1	299	.280729	.000008	.000725	.280683	.6	.28	.54
42984.1	42984-15.1	323	.280720	.000014	.000683	.280676	.0	.49	.54
42984.1	42984-17.1	297	.280695	.000012	.000762	.280647	0.7	.42	.60
42984.1	42984-19.1	325	.280687	.000011	.000434	.280659	.4	.39	.57
42984.1	42984-21.1	298	.280687	.000008	.000769	.280638	1.0	.29	.62
42984.1	42984-23.1	286	.280733	.000009	.000587	.280696	.8	.30	.52
42984.1	42984-25.1	337	.280704	.000010	.000714	.280658	.6	.35	.57

42984.1	42984-06.1	422	.280682	.000020	.001038	.280614	.1	.70	.62
42985.1	42985-01.1	295	.280761	.000014	.001443	.280670	.1	.49	.56
42985.1	42985-03.1	292	.280700	.000016	.000914	.280642	1.0	.56	.61
42985.1	42985-04.1	296	.280701	.000020	.000859	.280647	0.7	.70	.61
42985.1	42985-05.1	286	.280665	.000025	.000472	.280635	1.4	.88	.63
42985.1	42985-08.1	318	.280686	.000024	.001055	.280619	1.2	.84	.65
42985.1	42985-08.2	314	.280722	.000017	.001160	.280648	0.3	.60	.60
42985.1	42985-10.2	313	.280709	.000019	.001116	.280638	0.6	.67	.61
42985.1	42985-11.1	321	.280742	.000012	.000651	.280700	.8	.42	.50

42985.1	42985-15.1	312	.280724	.000019	.001239	.280645	0.4	.67	.60
42985.1	42985-18.1	308	.280684	.000020	.000551	.280649	0.4	.70	.60
42985.1	42985-21.1	274	.280715	.000017	.000777	.280666	0.6	.60	.58
69038.1	69038-01.1	312	.280665	.000015	.000449	.280636	0.7	.53	.62
69038.1	69038-03.1	319	.280619	.000011	.000366	.280596	2.0	.39	.69
69038.1	69038-05.1	315	.280644	.000022	.000520	.280611	1.6	.77	.66
69038.1	69038-07.1	312	.280663	.000013	.000548	.280628	1.0	.46	.63
69038.1	69038-09.1	315	.280662	.000009	.000314	.280642	0.5	.32	.61
69038.1	69038-13.1	318	.280679	.000010	.000290	.280660	.3	.35	.57

69038.1	69038-15.1	323	.280696	.000014	.000632	.280656	.2	.49	.58
69038.1	69038-17.1	315	.280641	.000008	.000401	.280615	1.4	.28	.65
69038.1	69038-20.1	305	.280655	.000011	.000362	.280632	1.0	.39	.63
69038.1	69038-21.1	308	.280651	.000012	.000468	.280621	1.4	.42	.65
69038.1	69038-22.1	313	.280657	.000012	.000568	.280621	1.3	.42	.65
69038.1	69038-23.1	325	.280699	.000010	.000845	.280645	0.1	.35	.60
69040.1	69040-03.1	315	.280833	.000034	.002383	.280681	.9	.19	.54
69040.1	69040-05.1	310	.280711	.000015	.000932	.280652	0.2	.53	.59
69040.1	69040-06.1	313	.280717	.000010	.000682	.280674	.6	.35	.55

69040.1	69040-11.1	302	.280723	.000013	.001806	.280608	2.0	.46	.67
69040.1	69040-13.1	374	.280686	.000011	.001245	.280605	0.4	.39	.65
69040.1	69040-16.1	340	.280701	.000006	.002057	.280569	2.5	.21	.73
69040.1	69040-07.1	432	.280620	.000008	.000657	.280577	.0	.27	.68
69042.1	69042-01.1	324	.280773	.000019	.001089	.280703	.9	.67	.49
69042.1	69042-07.1	310	.280700	.000034	.001400	.280611	1.7	.19	.66
69042.1	69042-13.1	316	.280650	.000023	.000567	.280614	1.4	.81	.66
69042.1	69042-16.1	307	.280754	.000010	.001077	.280686	.9	.35	.53
69042.1	69042-17.1	313	.280695	.000020	.001663	.280589	2.4	.70	.70

69042.1	69042-21.1	323	.280765	.000010	.001460	.280672	.8	.35	.55
69042.1	69042-02.1	457	.280670	.000013	.001592	.280564	.1	.46	.69
69042.1	69042-04.1	468	.280759	.000018	.002435	.280596	.5	.63	.63
69042.1	69042-05.1	458	.280668	.000017	.002110	.280527	1.2	.60	.76
69042.1	69042-06.1	451	.280651	.000020	.001507	.280551	0.5	.70	.72
69042.1	69042-09.1	466	.280686	.000018	.001691	.280573	.6	.63	.67
69042.1	69042-11.1	462	.280717	.000014	.002067	.280579	.8	.49	.66
69042.1	69042-12.1	462	.280712	.000015	.001443	.280616	.1	.53	.60
69042.1	69042-19.1	465	.280698	.000011	.001542	.280595	.4	.39	.63

69042.1	69042-20.1	476	.280675	.000022	.000745	.280625	.7	.77	.57
69045.1	69045-02.1	310	.280736	.000010	.000716	.280690	.2	.35	.52
69045.1	69045-04.1	314	.280724	.000013	.001153	.280650	0.2	.46	.59
69045.1	69045-09.1	310	.280741	.000011	.000988	.280678	.7	.39	.54
69045.1	69045-13.1	306	.280747	.000011	.001287	.280665	.2	.39	.57
69045.1	69045-15.1	306	.280735	.000010	.000780	.280685	.9	.34	.53
69045.1	69045-18.1	308	.280746	.000009	.001036	.280680	.7	.31	.54
69045.1	69045-20.1	314	.280785	.000012	.000921	.280726	.5	.42	.45
69045.1	69045-21.1	307	.280733	.000015	.000503	.280701	.5	.53	.50

69045.1	69045-23.1	310	.280731	.000007	.000976	.280669	.4	.23	.56
69045.1	69045-26.1	309	.280717	.000009	.000749	.280669	.4	.33	.56
69046.1	69046-02.1	309	.280740	.000016	.001161	.280666	.3	.56	.56
69046.1	69046-03.1	317	.280699	.000020	.001079	.280630	0.8	.70	.63
69046.1	69046-05.1	317	.280688	.000016	.000664	.280646	0.3	.56	.60
69046.1	69046-07.1	308	.280676	.000028	.000701	.280631	1.0	.98	.63
69046.1	69046-09.1	317	.280738	.000023	.002213	.280597	2.0	.81	.69
69046.1	69046-11.1	314	.280739	.000017	.000920	.280680	.9	.60	.54
69046.1	69046-12.2	298	.280770	.000020	.001157	.280697	.1	.70	.51

69046.1	69046-13.1	298	.280744	.000013	.001434	.280653	0.5	.46	.59
69046.1	69046-19.1	288	.280673	.000018	.001094	.280604	2.4	.63	.69
78037.1	78037-02.1	318	.280747	.000011	.001459	.280654	.0	.39	.58
78037.1	78037-04.1	317	.280687	.000082	.001207	.280610	1.5	.87	.66
78037.1	78037-08.1	313	.280678	.000028	.001072	.280610	1.6	.98	.67
78037.1	78037-09.1	311	.280706	.000022	.000747	.280658	.0	.77	.58
78037.1	78037-11.1	312	.280714	.000035	.001482	.280620	1.3	.23	.65
78037.1	78037-14.1	315	.280697	.000012	.001641	.280592	2.2	.42	.70
78037.1	78037-16.1	309	.280655	.000028	.001592	.280554	3.7	.98	.77

78037.1	78037-19.1	299	.280733	.000010	.000518	.280700	.2	.35	.51
78037.1	78037-21.1	315	.280702	.000013	.000491	.280671	.6	.46	.55
78075.1	78075-01.1	303	.280685	.000011	.000634	.280645	0.6	.39	.61
78075.1	78075-02.1	300	.280686	.000012	.000780	.280637	1.0	.42	.62
78075.1	78075-03.1	306	.280671	.000010	.000495	.280640	0.7	.35	.61
78075.1	78075-06.1	296	.280663	.000009	.000431	.280636	1.1	.31	.62
78075.1	78075-08.1	308	.280686	.000015	.000420	.280659	.0	.53	.58
78075.1	78075-11.1	311	.280722	.000013	.000701	.280677	.7	.46	.54
78075.1	78075-16.1	310	.280695	.000007	.000342	.280673	.5	.23	.55

78075.1	78075-17.1	306		.280698	.000011	.000421	.280671	.4	.39	.56
78075.1	78075-19.1	308		.280722	.000011	.000376	.280698	.4	.39	.51
78075.1	78075-21.1	296		.280668	.000012	.000208	.280655	0.4	.42	.59
78075.1	78075-24.1	297		.280720	.000018	.000526	.280687	.7	.63	.53
78075.1	78075-14.1	413		.280764	.000018	.000983	.280699	.9	.63	.46
78075.1	78075-18.1	445		.280624	.000010	.000554	.280587	.7	.35	.66
78077.1	78077-01.1	314		.280737	.000032	.000696	.280693	.3	.12	.51
78077.1	78077-03.1	323	1	.280747	.000009	.000648	.280706	.0	.32	.49
78077.1	78077-05.1	307		.280712	.000014	.000401	.280686	.9	.49	.53

78077.1	78077-07.1	313	.280719	.000029	.000566	.280683	.0	.02	.53
78077.1	78077-08.1	320	.280693	.000018	.000668	.280650	.0	.63	.59
78077.1	78077-10.1	323	.280789	.000012	.000478	.280758	.9	.42	.39
78077.1	78077-12.1	323	.280741	.000012	.000517	.280708	.1	.42	.48
78077.1	78077-18.1	310	.280719	.000012	.000575	.280682	.9	.42	.53
78077.1	78077-20.1	322	.280750	.000012	.000714	.280704	.9	.42	.49
78077.1	78077-21.1	314	.280706	.000013	.000444	.280678	.8	.46	.54
78077.1	78077-22.1	317	.280722	.000010	.000534	.280688	.2	.34	.52
78077.1	78077-23.1	308	.280710	.000010	.000462	.280681	.8	.35	.54

78077.1	78077-24.1	313		.280724	.000014	.000595	.280686	.1	.49	.53
78095.1	78095-02.2	346		.280705	.000023	.000725	.280658	.9	.81	.56
78095.1	78095-03.1	309		.280567	.000028	.000750	.280519	5.0	.98	.83
78095.1	78095-08.1	308	6	.280718	.000013	.000821	.280666	.2	.46	.57
78095.1	78095-14.2	309		.280694	.000018	.000845	.280640	0.7	.63	.61
78095.1	78095-14.3	312		.280786	.000024	.000876	.280730	.6	.84	.45
78095.1	78095-14.4	302		.280723	.000023	.000889	.280667	.1	.81	.57
78095.1	78095-02.3	412		.280693	.000027	.000886	.280635	.6	.95	.58
78095.1	78095-11.1	432		.280626	.000010	.000458	.280596	.6	.35	.65

78095.1	78095-11.2	427		.280617	.000010	.000436	.280588	.3	.34	.66
78096.1	78096-05.1	307		.280771	.000028	.001205	.280694	.2	.98	.51
78096.1	78096-06.1	283	0	.280727	.000020	.001150	.280654	0.8	.70	.60
78096.1	78096-08.1	302		.280728	.000015	.001115	.280657	0.2	.53	.58
78096.1	78096-10.1	307	8	.280686	.000015	.000508	.280654	0.2	.53	.59
78096.1	78096-12.1	323	1	.280735	.000026	.001009	.280671	.8	.91	.55
78096.1	78096-14.1	298		.280774	.000017	.001266	.280694	.0	.60	.52
78096.1	78096-15.1	288		.280722	.000013	.000570	.280686	.5	.46	.54
78096.1	78096-16.1	307		.280691	.000015	.001400	.280602	2.1	.53	.68

78096.1	78096-19.1	302	.280740	.000026	.000923	.280681	.6	.91	.54
78096.1	78096-21.1	281	.280744	.000025	.001439	.280653	0.8	.88	.60
78096.1	78096-22.1	283	.280760	.000021	.001367	.280674	0.1	.74	.56
78096.1	78096-23.1	299	.280726	.000011	.001372	.280639	0.9	.39	.62
78098.1	78098-01.1	303	.280687	.000022	.000479	.280657	0.2	.77	.58
78098.1	78098-02.1	301	.280783	.000079	.000656	.280741	.8	.77	.43
78098.1	78098-05.1	307	.280633	.000049	.000450	.280604	2.0	.72	.68
78098.1	78098-08.1	291	.280741	.000019	.001251	.280662	0.3	.67	.58
78098.1	78098-11.1	305	.280702	.000026	.001043	.280636	0.9	.91	.62

78098.1	78098-12.1	296	.280728	.000020	.000876	.280672	.2	.70	.56
78098.1	78098-13.1	302	.280766	.000014	.000947	.280706	.5	.49	.50
78098.1	78098-15.1	300	.280782	.000017	.000970	.280720	.0	.60	.47
78098.1	78098-17.1	299	.280771	.000040	.000555	.280736	.5	.40	.44
78098.1	78098-19.1	307	.280710	.000026	.000953	.280649	0.4	.91	.60
78098.1	78098-21.1	295	.280742	.000027	.001412	.280653	0.5	.95	.59
78098.1	78098-23.1	290	.280773	.000012	.001072	.280705	.2	.42	.50
78098.1	78098-25.1	294	.280736	.000012	.000776	.280687	.7	.42	.53
78099.1	78099-01.1	284	.280697	.000012	.000708	.280652	0.8	.42	.60

78099.1	78099-02.1	304	.280742	.000020	.000499	.280710	.7	.70	.49
78099.1	78099-06.1	310	.280738	.000011	.000701	.280693	.3	.39	.51
78099.1	78099-08.1	310	.280705	.000036	.001314	.280621	1.3	.26	.65
78099.1	78099-11.1	306	.280733	.000012	.000410	.280707	.7	.42	.49
78099.1	78099-12.1	293	.280749	.000012	.000712	.280704	.2	.42	.50
78099.1	78099-13.1	315	.280745	.000015	.000585	.280708	.9	.53	.49
78099.1	78099-16.1	309	.280711	.000015	.000652	.280669	.4	.53	.56
78099.1	78099-18.1	308	.280734	.000011	.000594	.280696	.3	.39	.51

Tambina

Supersuite

69031.1	69031-04.1	425		.280620	.000033	.001237	.280538	1.6	.16	.75
69031.1	69031-08.1	428		.280637	.000021	.000762	.280587	.2	.74	.66
69031.1	69031-10.1	447		.280731	.000034	.002722	.280550	0.6	.19	.72
69031.1	69031-12.1	435		.280665	.000038	.000989	.280600	.9	.33	.64
69031.1	69031-18.1	429		.280828	.000023	.002407	.280669	.2	.81	.51
69031.1	69031-20.1	425		.280701	.000015	.001296	.280616	.2	.53	.61
69031.1	69031-22.1	426		.280755	.000015	.002085	.280617	.3	.53	.61
69031.1	69031-23.1	435	0	.280724	.000014	.001781	.280606	.1	.49	.62
69031.1	69031-24.1	425		.280748	.000013	.001812	.280628	.7	.46	.59

69041.1	69041-10.1	316		.280689	.000016	.002012	.280561	3.3	.56	.75
69041.1	69041-05.1	468		.280677	.000008	.001607	.280570	.6	.29	.68
69041.1	69041-08.1	463		.280734	.000013	.001966	.280603	.6	.46	.62
69041.1	69041-12.1	461		.280747	.000010	.002265	.280596	.3	.35	.63
69041.1	69041-15.1	434		.280680	.000008	.002071	.280543	1.2	.27	.74
69041.1	69041-16.1	425		.280662	.000010	.001146	.280586	.2	.35	.66
78036.1	78036-01.1	437		.280695	.000010	.000450	.280665	.2	.35	.52
78036.1	78036-02.1	459	0	.280577	.000014	.000757	.280527	1.2	.49	.76
78036.1	78036-03.1	436		.280676	.000020	.001361	.280586	.4	.70	.66

78036.1	78036-03.2	438	.280715	.000018	.000826	.280660	.1	.63	.53
78036.1	78036-04.1	481	.280676	.000018	.001177	.280597	.9	.63	.62
78036.1	78036-07.2	448	.280619	.000017	.000635	.280577	.4	.60	.67
78036.1	78036-08.1	459	.280593	.000015	.001268	.280509	1.8	.53	.79
78036.1	78036-13.1	468	.280653	.000021	.000855	.280596	.5	.74	.63
78036.1	78036-13.2	455	.280727	.000013	.001801	.280607	.6	.46	.62
78036.1	78036-15.1	431	.280715	.000015	.001595	.280610	.1	.53	.62
78079.1	78079-01.1	408	.280742	.000033	.002254	.280594	.0	.16	.66
78079.1	78079-03.1	406	.280711	.000030	.001684	.280601	.2	.05	.65

78079.1	78079-04.1	449	4	.280702	.000021	.001106	.280629	.2	.74	.58
78079.1	78079-04.2	466	2	.280666	.000020	.000878	.280607	.9	.70	.61
78079.1	78079-06.1	421		.280742	.000030	.001776	.280625	.4	.05	.60
78079.1	78079-11.1	454		.280696	.000017	.001465	.280599	.3	.60	.63
78079.1	78079-11.2	467		.280654	.000017	.001334	.280565	.4	.60	.69
78079.1	78079-16.1	454		.280600	.000017	.000862	.280543	0.7	.60	.73
78100.1	78100-02.1	434		.280740	.000020	.002012	.280607	.1	.70	.62
78100.1	78100-10.1	469		.280755	.000014	.002068	.280617	.3	.49	.59
78100.1	78100-11.1	428		.280675	.000013	.001350	.280586	.2	.46	.66

78100.1	78100-12.1	435		.280779	.000011	.002102	.280640	.3	.39	.56
78100.1	78100-13.1	433		.280768	.000013	.002441	.280607	.1	.46	.62
78100.1	78100-14.1	446	9	.280733	.000011	.001330	.280645	.7	.39	.55
Split Rock Supersuite										
69044.1	69044-04.1	887		.280974	.000039	.002060	.280860	2.7	.37	.37
69044.1	69044-08.1	837		.280878	.000022	.001065	.280820	5.3	.77	.46
69044.1	69044-08.4	832		.280975	.000020	.000599	.280943	1.0	.70	.24
69044.1	69044-09.1	833		.280939	.000020	.000698	.280901	2.5	.70	.32
69044.1	69044-09.3	822	2	.280908	.000020	.001620	.280820	5.6	.70	.47

69044.1	69044-09.4	819	3	.280908	.000013	.002148	.280792	6.7	.46	.52
69044.1	69044-02.1	433		.280610	.000017	.000496	.280577	.0	.60	.68

ample ID	Super suite	ge Ma)	$^{47}Sm/^{144}Nd$ meas)	$^{43}Nd/^{144}Nd$ meas)	σ	$^{43}Nd/^{144}Nd$ initial	Nd	$_{DM}^{2}$ (Ga)
	Mount Edgar Dome							
	Split						(	
69044	Rock Supersuite	831 ± 12	.2178	.512685		.508614	7.08	.65
	Emu						(	
69042	Pool Supersuite	323 ± 9	.0900	.510242		.508272	1.44	.63
	Tambi						(	
78036	na Supersuite	435 ± 4	.1086	.510646		.508180	0.03	.63
	Tambi						(	
69041	na Supersuite	466 ± 4	.1247	.511039		.508212	.40	.59
	Muccan Dome							
	Callina						(	

42828	Supersuite	470 ± 4	.0974	.510357	.508122	0.26	.67
	Shaw Dome						
	Sisters						
42967	Supersuite	929 ± 5	.0783	.510105	.508592	4.99	.58

- We present new Hf and Nd data from the Mount Edgar Dome, East Pilbara Terrane
- These chart the Palaeo-Mesoarchaean magmatic evolution of a single granite complex
- Reworking of existing TTG crust dominated late Palaeoarchaean magmatism
- This trend supports a vertical tectonic geodynamic regime >3.2 Ga for the Pilbara
- The data further support a cryptic >3.5Ga protocrust of unknown extent

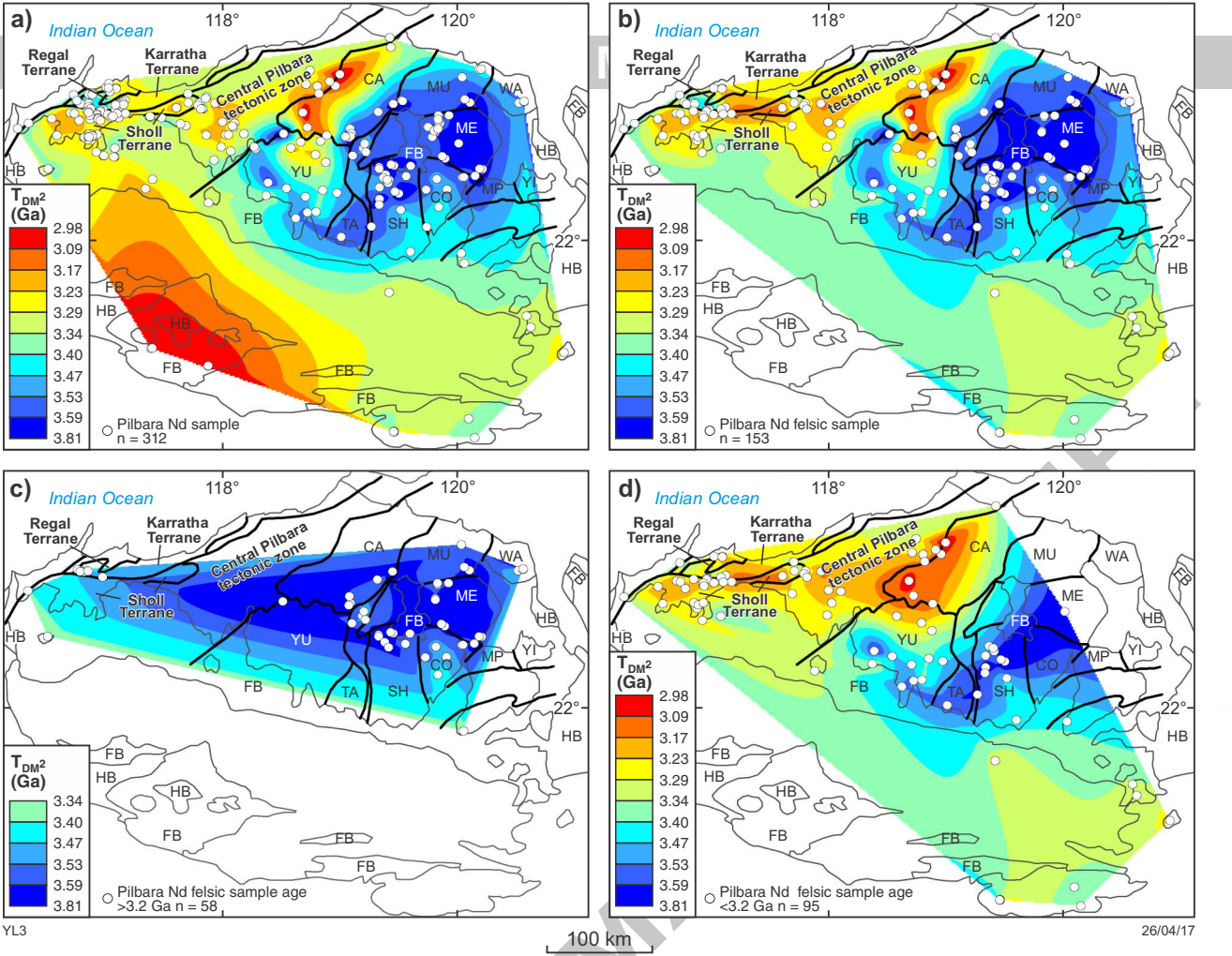
a)
Indian Ocean
118°
120°
Regal Terrane
Karratha Terrane
Central Pilbara tectonic zone
Sholl Terrane
CA
MU
WA
ME
FB
HB
YU
CO
MP
YI
TA
SH
22°
T_{DM}^2 (Ga)
2.98
3.09
3.17
3.23
3.29
3.34
3.40
3.47
3.53
3.59
3.81
Pilbara Nd sample
n = 312
b)
Pilbara Nd felsic sample
n = 153
c)
Pilbara Nd felsic sample age
>3.2 Ga n = 58
d)
Pilbara Nd felsic sample age
<3.2 Ga n = 95
100 km

YL3

26/04/17

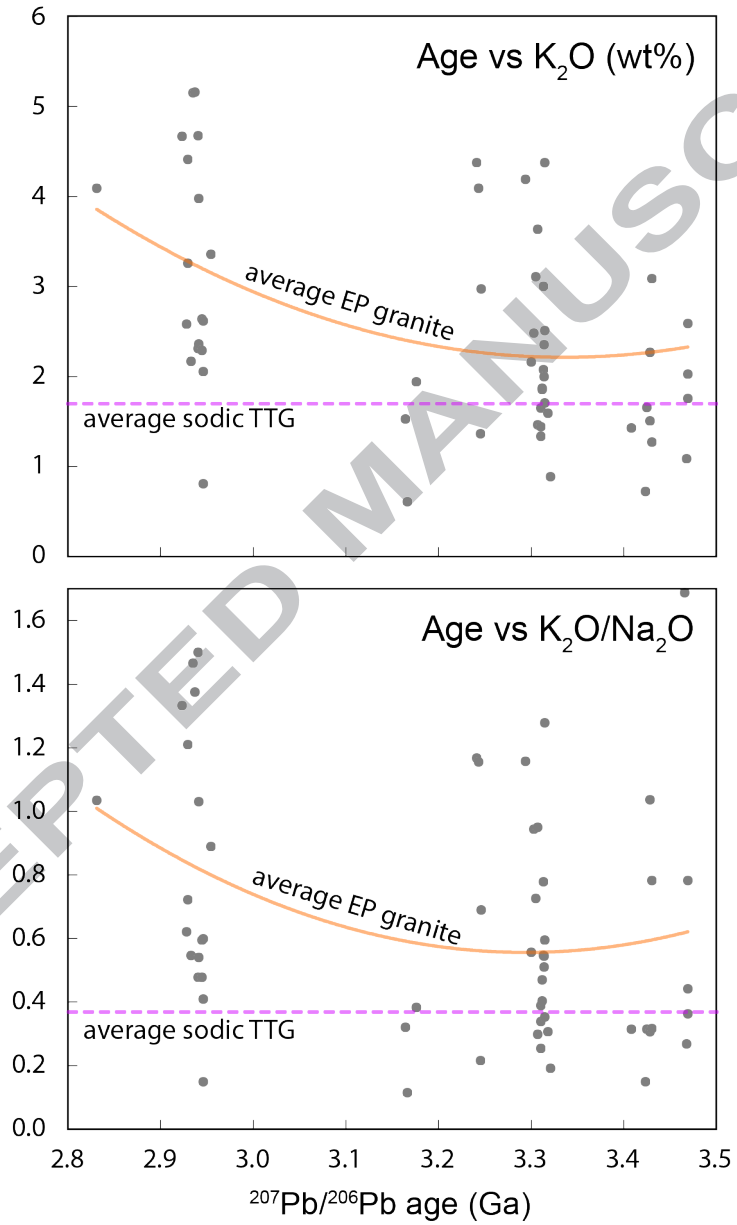

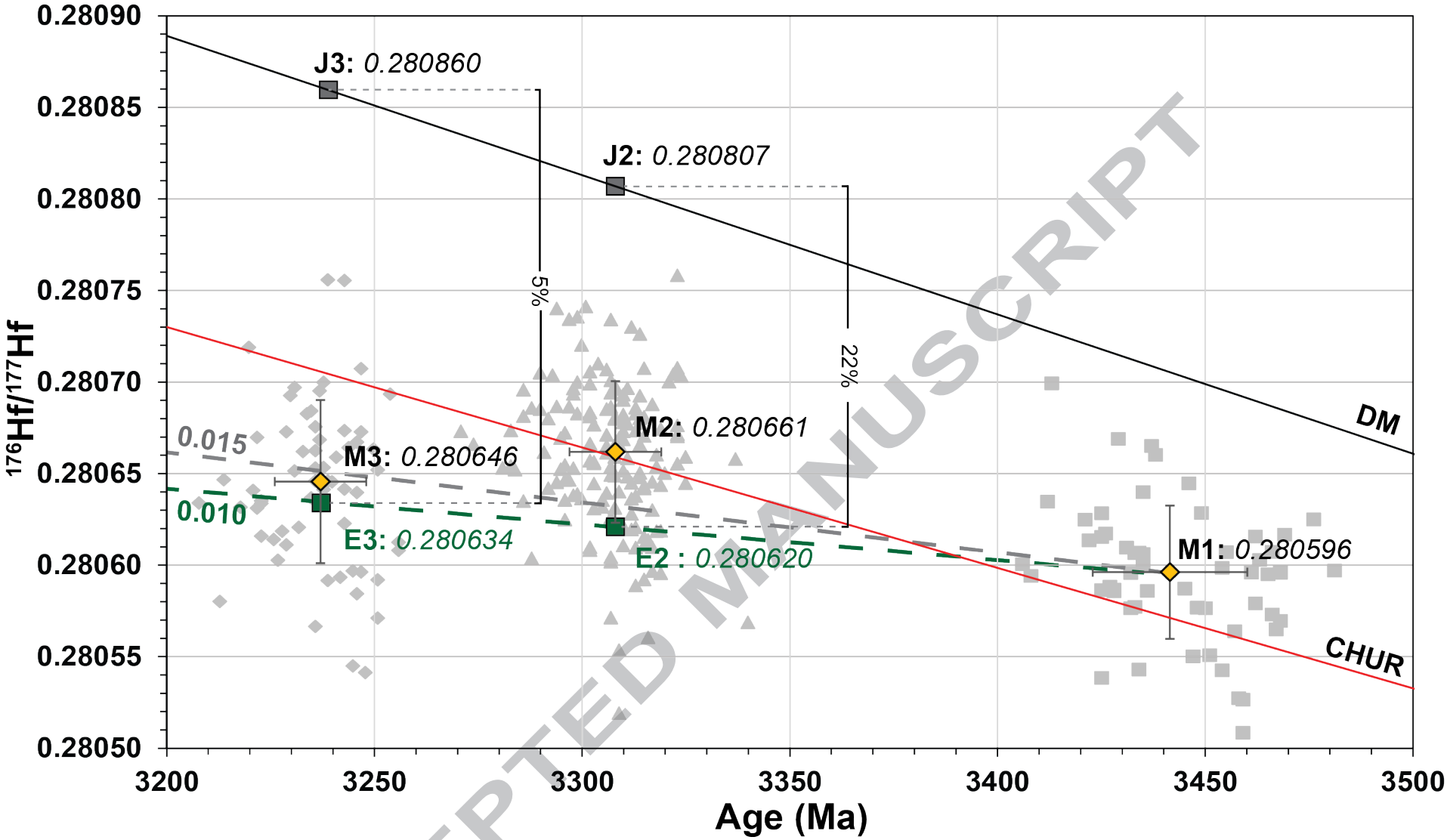

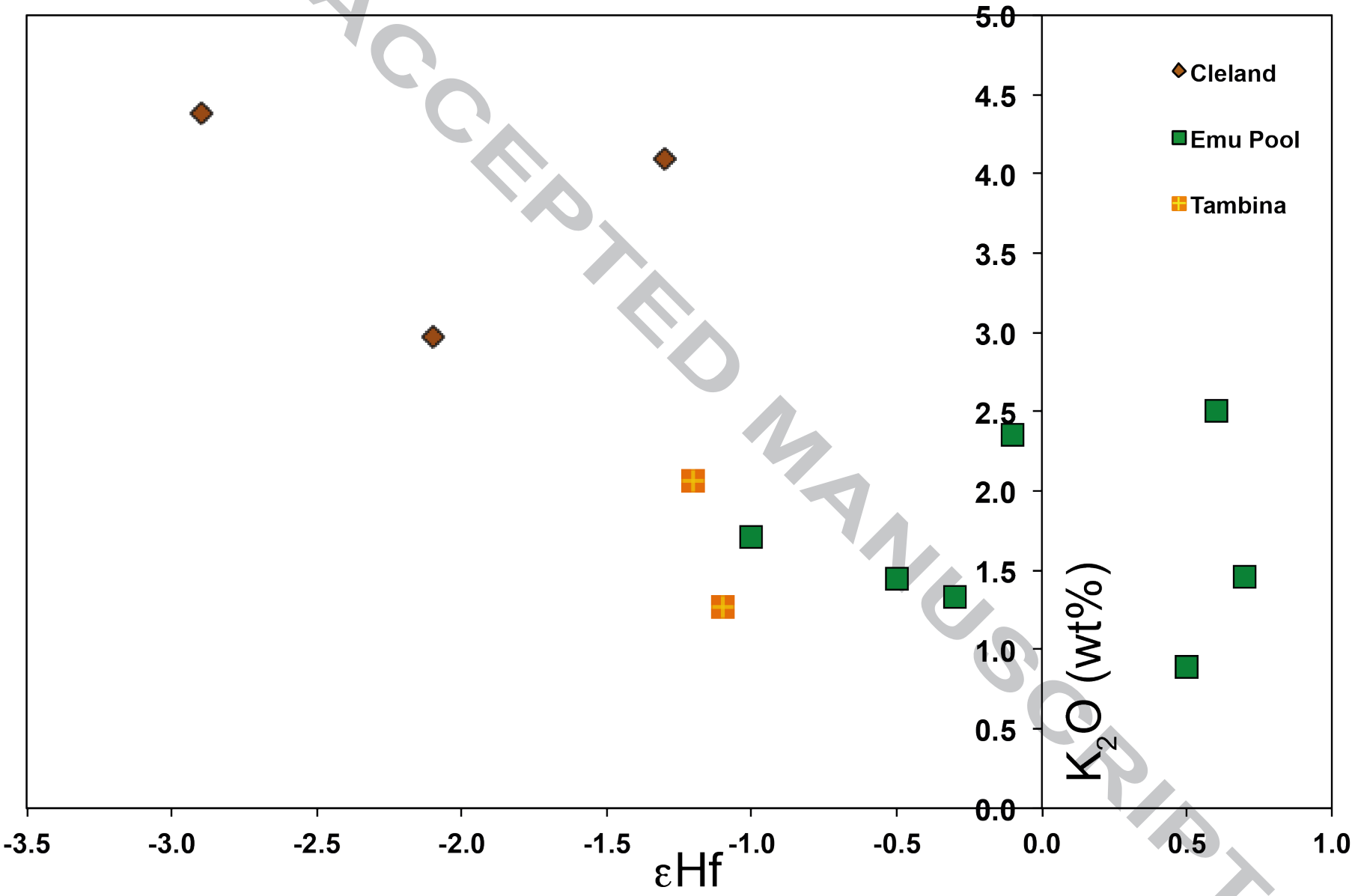

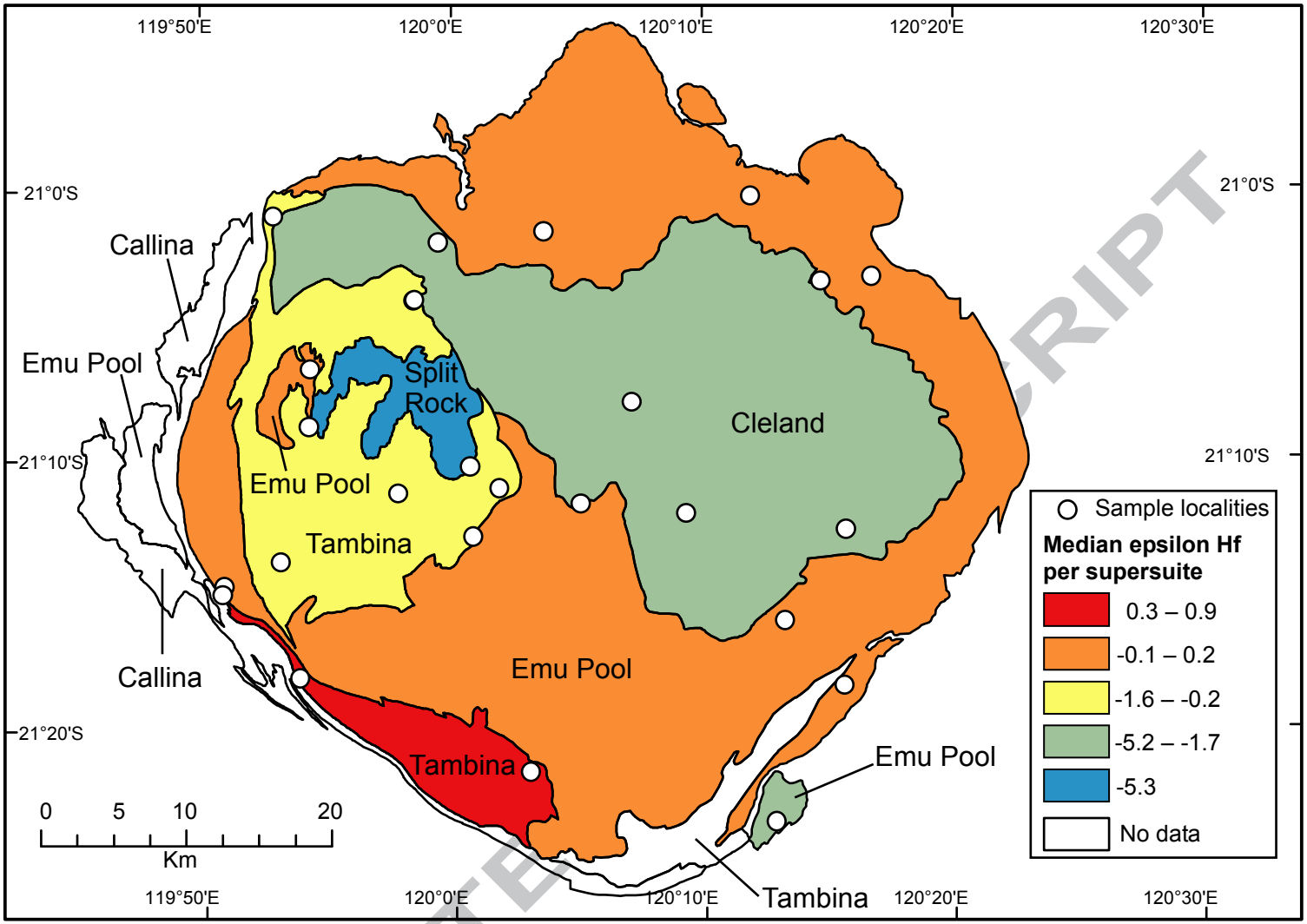

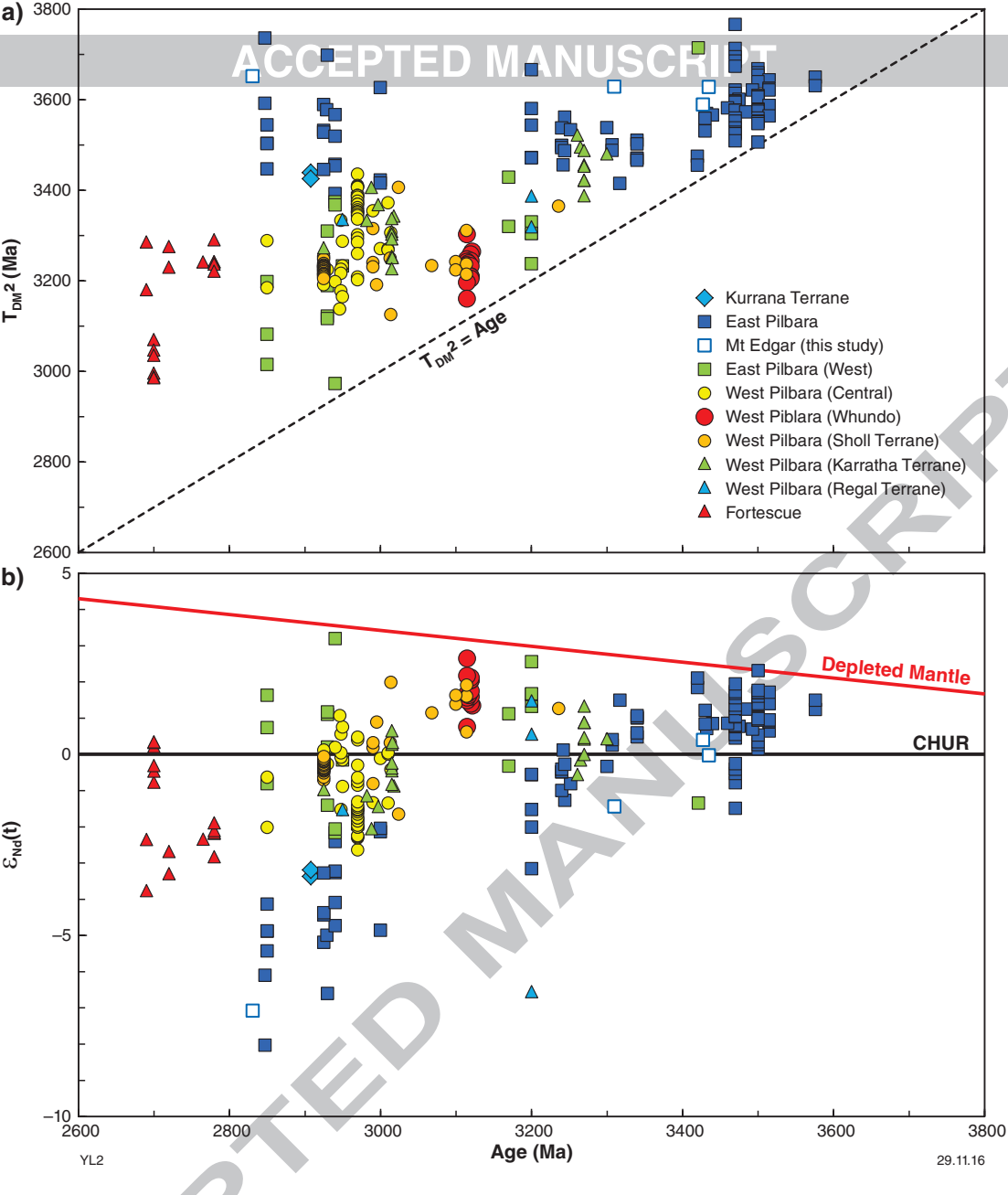

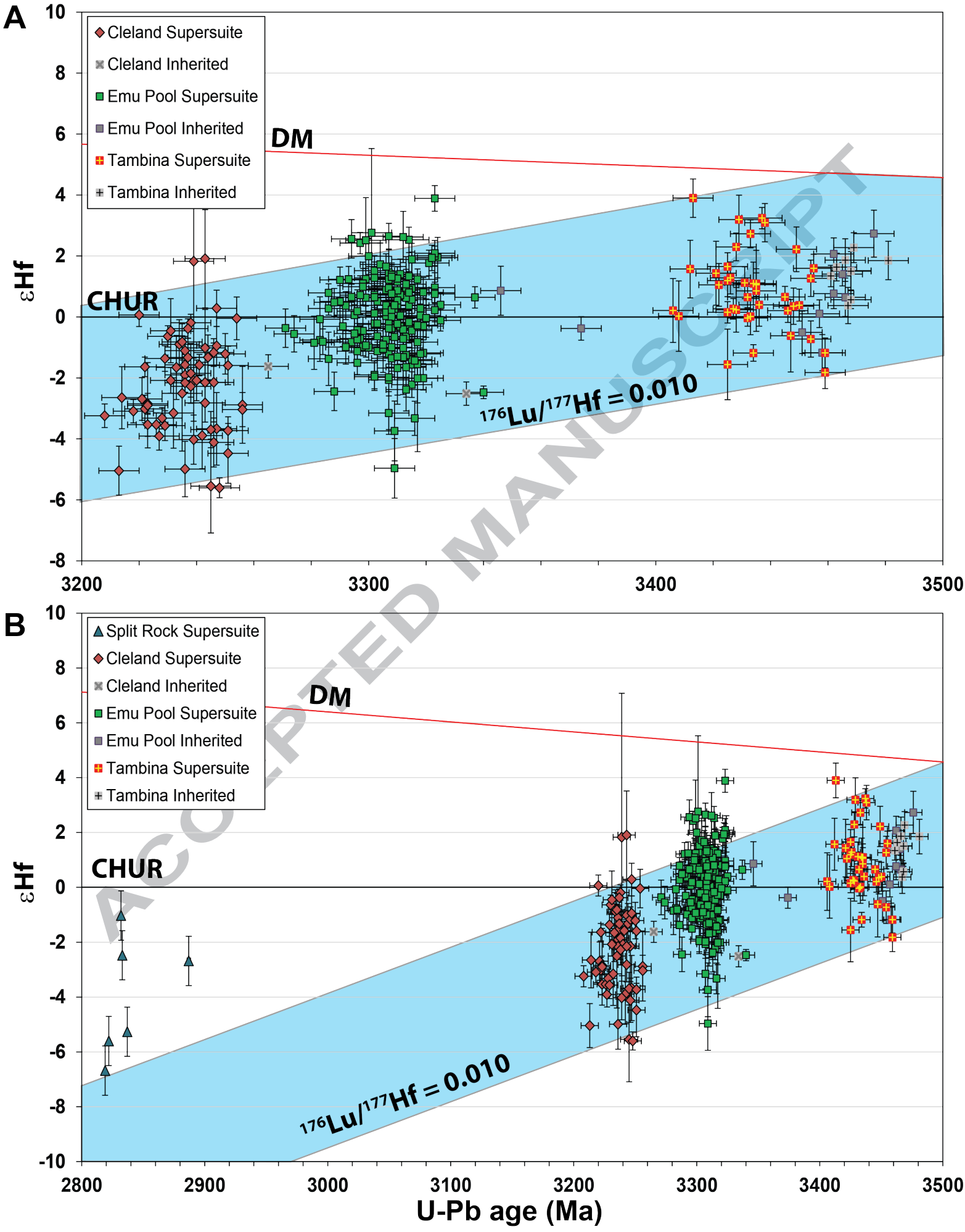

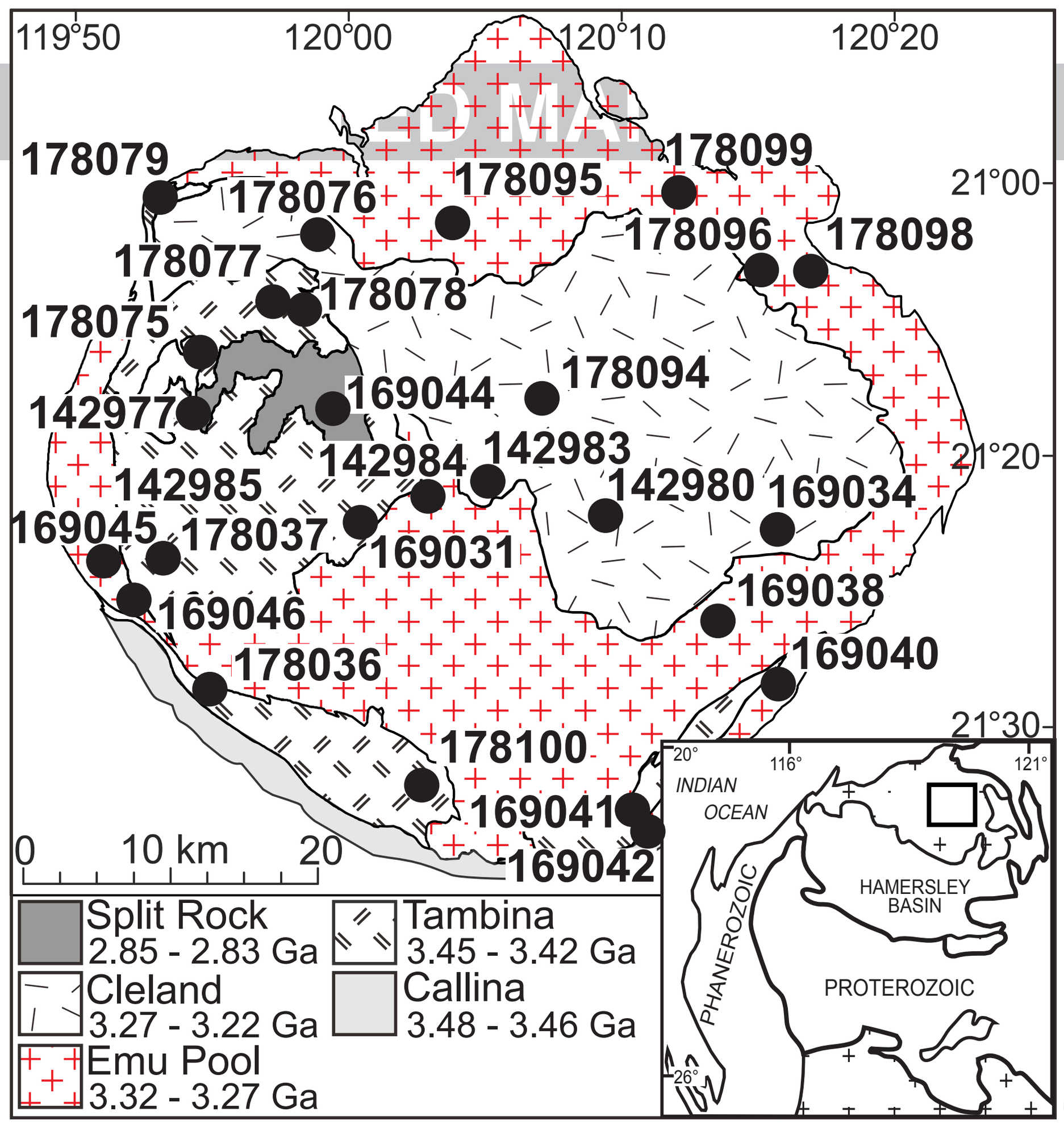
119°50
120°00
120°10
120°20
21°00
21°20
21°30
178079
178076
178095
178099
178096
178098
178077
178078
178075
178094
169044
142977
142983
142984
142985
142980
169034
169045
178037
169031
169038
169046
178036
169040
178100
169041
169042
0
10 km
20
Split Rock
2.85 - 2.83 Ga
Tambina
3.45 - 3.42 Ga
Cleland
3.27 - 3.22 Ga
Callina
3.48 - 3.46 Ga
Emu Pool
3.32 - 3.27 Ga
20°
116°
121°
INDIAN
OCEAN
PHANEROZOIC
HAMERSLEY
BASIN
PROTEROZOIC
26°

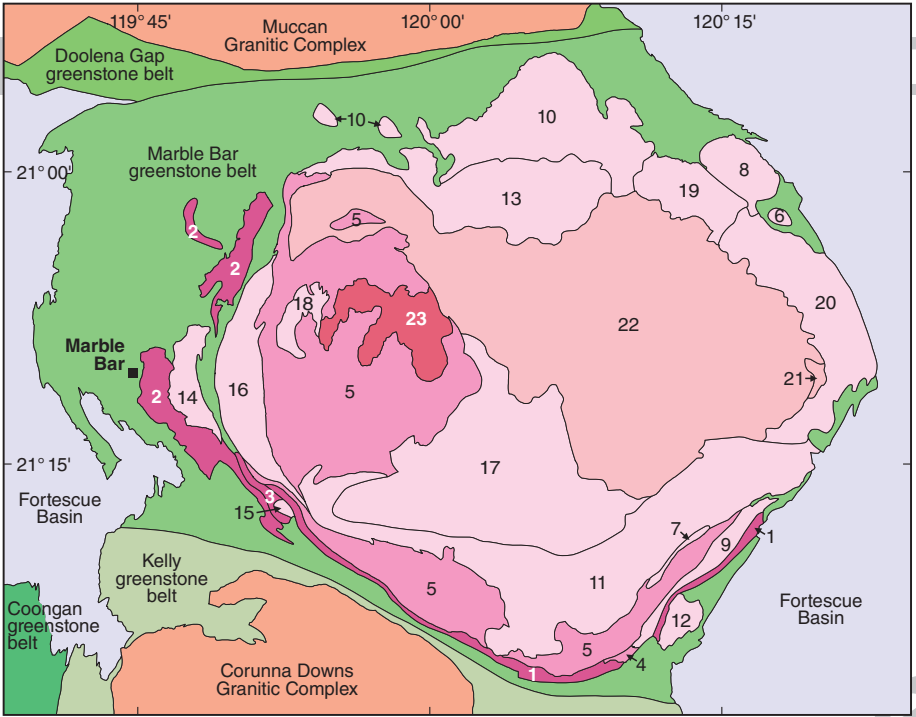

Split Rock Supersuite (2851–2831 Ma)
- 23 Moolyella Monzogranite

Cleland Supersuite (3274–3223 Ma)
- 22 Bishop Creek Monzogranite
- 21 Bullgarina Monzogranite

Emu Pool Supersuite (3324–3277 Ma)
- 20 Zulu Granodiorite
- 19 Mullugunya Granodiorite
- 18 Johansen Monzogranite
- 17 Joorina Granodiorite
- 16 Jenkin Granodiorite
- 15 Cotton Well Granodiorite
- 14 Campbell Granodiorite
- 13 Munganbrina Monzogranite
- 12 Wilina Granodiorite
- 11 Kennell Granodiorite
- 10 Coppin Gap Granodiorite
- 9 Chessman Granodiorite
- 8 Chimingadgi Trondhjemite
- 7 Davitt Syenogranite
- 6 Walgunyah Trondhjemite

Tambina Supersuite (3451–3416 Ma)
- 5 Fig Tree Gneiss
- 4 Lady Adelaide Orthogneiss

Callina Supersuite (3484–3462 Ma)
- 3 Owens Gully Diorite
- 2 Homeward Bound Granite
- 1 Underwood Gneiss

20 km

AHH686

22.06.16

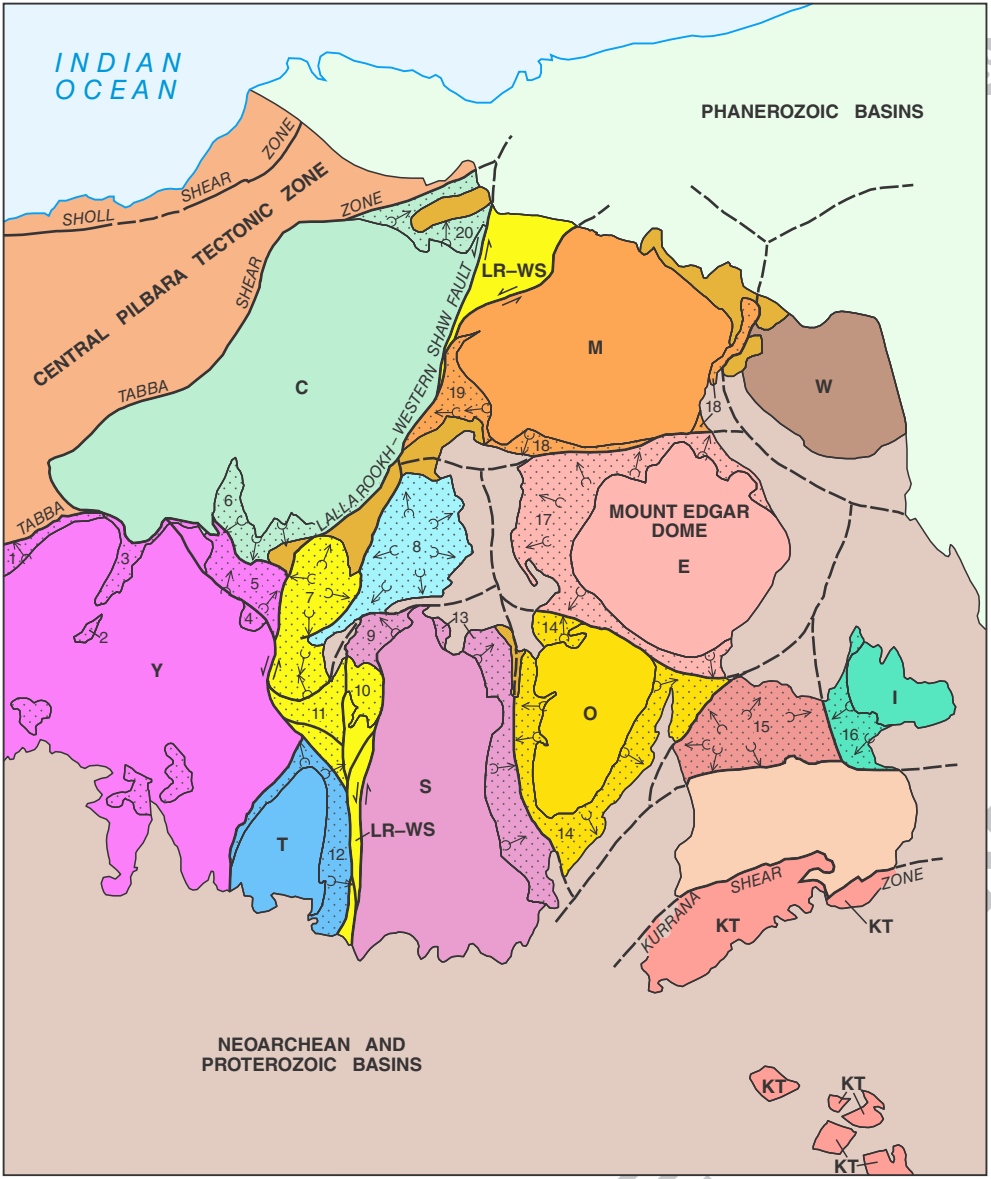

SCRIPT

Lalla Rookh – Western Shaw Structural Corridor

LR–WS Granitic Rocks

Greenstone belts
7 Soanesville
10 Emerald Mine
11 Tambina

De Grey Superbasin

Mosquito Creek Basin

KT Kurrana Terrane

Dome name:	Granitic complex	Greenstone belt
Carlindi	C	6 East Strelley 20 Goldsworthy
Corunna Downs	O	14 Kelly
McPhee	not exposed	15 McPhee
Mount Edgar	E	17 Marble Bar
Muccan	M	18 Doolena Gap 19 Warralong
North Pole	not exposed	8 Panorama
Shaw	S	9 North Shaw 13 Coongan
Tambourah	T	12 Western Shaw
Warrawagine	W	not exposed
Yilgalong	I	16 Mount Elsie
Yule	Y	1 Pilbara Well 2 Mount Francisco 3 Wodgina 4 Abydos 5 Pincunah

Major fault or shear zone

Major fault or shear zone; inferred, concealed

Major fault or shear zone; showing relative sinistral displacement

Way-up from pillow structures

50 km

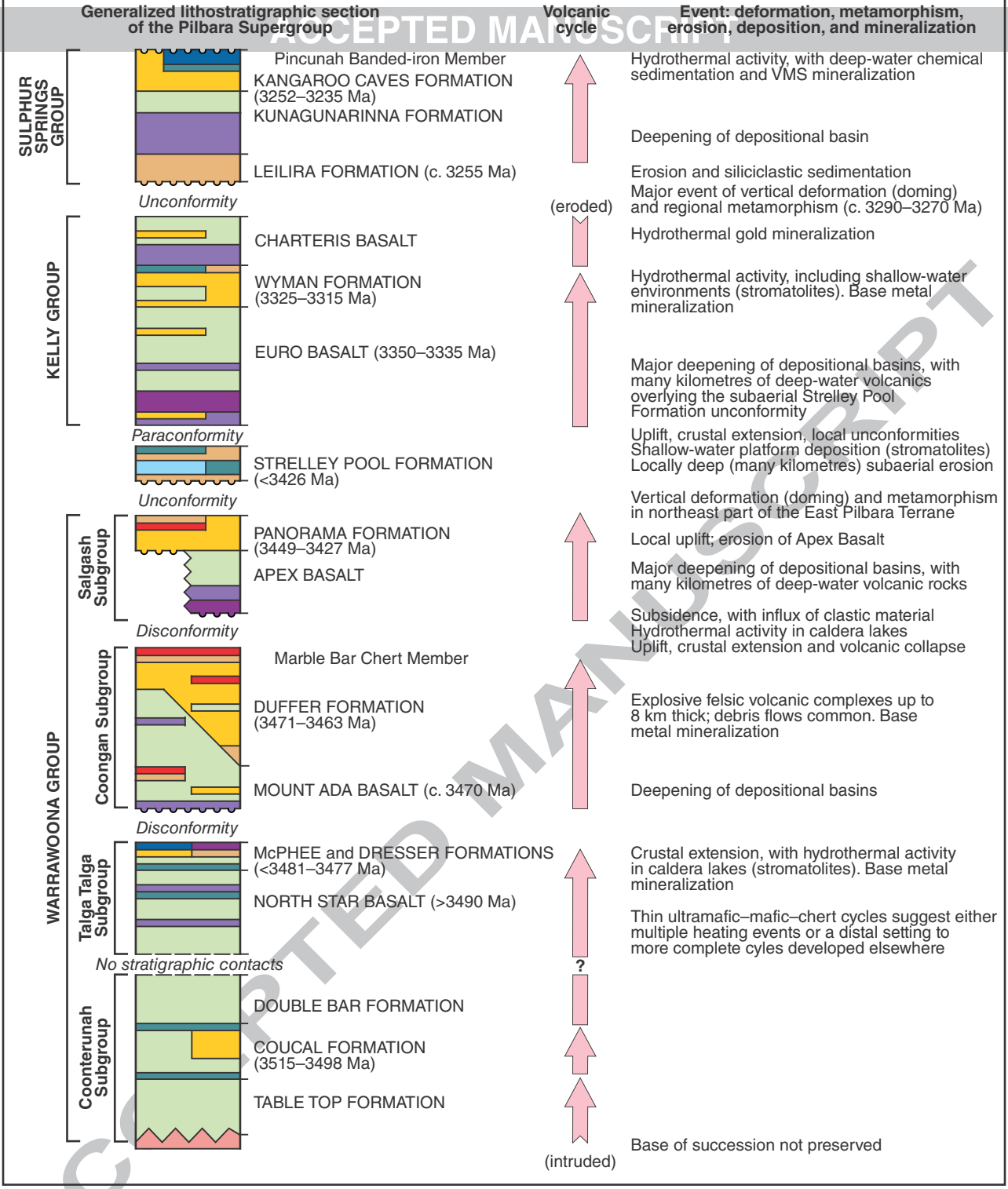

AHH419a

13/03/17

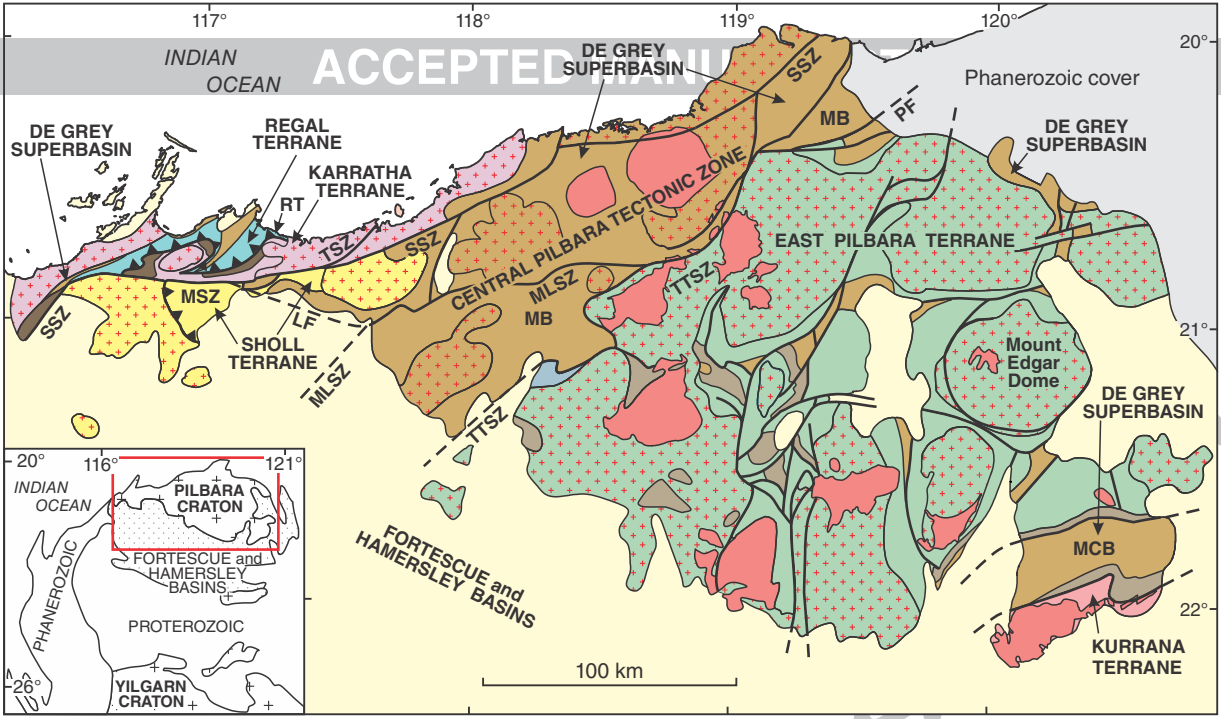

AHH660

14/03/17

Split Rock Supersuite

DE GREY SUPERBASIN

Granitic rocks intruding De Grey Supergroup

De Grey Supergroup: sedimentary and volcanic rocks

Regional Unconformity, c. 3066 Ma

WEST PILBARA SUPERTERRANE

Sholl Terrane

Granitic rocks intruding terrane

MSZ *Maitland Shear Zone*

Whundo Group: volcanic rocks

SSZ *Sholl Shear Zone*

Regal Terrane

Regal Formation: pillow basalt

RT *Regal Thrust*

Nickol River Basin

Nickol River Formation: sedimentary rocks

Soanesville Basin (volcanic section)

Honeyeater Basalt: pillow basalt

Soanesville Basin (lower sedimentary section) and similar basins

Clastic sedimentary rocks and BIF

Regional Unconformity, c. 3220 Ma

Karratha Terrane

Granitic rocks intruding terrane

Roebourne Group: volcanic rocks

East Pilbara Terrane

Granitic rocks intruding terrane

Pilbara Supergroup: predominantly volcanic rocks